Received: 15 June 2021 | Revised: 18 May 2022 | Accepted: 10 July 2022

DOI: 10.1002/rob.22109

SURVEY ARTICLE

WILEY

Gas source localization and mapping with mobile robots: A review

Adam Francis[1] | Shuai Li[1] | Christian Griffiths[2] | Johann Sienz[2]

[1]Department of Mechanical Engineering, Faculty of Science and Engineering, Swansea University, Swansea, UK

[2]Department of General Engineering, Faculty of Science and Engineering, Swansea University, Swansea, UK

Correspondence
Shuai Li, Department of Mechnical Engineering, Faculty of Science and Engineering, Swansea University, Swansea SA1 8EN, UK.
Email: shuai.li@swansea.ac.uk

Funding information
Engineering and Physical Sciences Research Council

Abstract

Within the last couple of decades, there has been increasing research into the use of mobile robots for gas sensing applications. This has led to many different branches of research, most notably on the topics of gas distribution mapping and source localization. This paper aims to provide an up to date and comprehensive overview of the research on these topics for both controlled and uncontrolled environments with ground-based or aerial robots. To complement other review papers, a greater focus is placed on recent probabilistic algorithms developed for both single robot and multirobot applications.

KEYWORDS
E-nose, gas discrimination, gas distribution mapping, gas source localization, mobile robot olfaction

1 | INTRODUCTION

In a modern world, understanding the chemical composition of the air around us is seen as a task of vital importance. Air monitoring is crucial for ensuring that the air we breathe is safe, and that air pollution levels are low for the sake of the environment. This is usually achieved by using air monitoring stations (Mooney et al., 2006), which are fixed devices often located on poles or beacons in areas where pollution is likely, such as near busy roads or industrial sites. Within industry, chemical sensors are mandatory in situations where flammable gas leaks may occur, such as in chemical and petrochemical plants. Undetected leaks can cause the build-up of large amounts of flammable gas, often leading to an explosion with the potential to harm large amounts of people. Body-worn detectors are commonplace to alert personnel of any direct exposure to potentially dangerous gases, and hand-held detectors are used to find the source location of leaks. Hand-held detectors bring their own drawbacks, such as the obvious safety risk to the operator from being in close proximity to potentially toxic and flammable chemicals.

Alternatively, mobile robots fitted with chemical sensors can be used to locate gas sources. Due to their mobile nature, only a single gas sensing device must be used to sample different locations, providing a greater resolution of measurements over a target area when compared to static sensors. Furthermore, they completely mitigate risk to human operators. This is a relatively modern application for robotics, as the subject has only been actively researched since the 1990s. Early research was generally focused on the development of chemical gradient following algorithms for locating the source of gas plumes (Rozas et al., 1991). Such approaches would use chemical sensors on the left and right side of the robot to track the plume, however, could not cope with turbulent conditions. Since then, more complex probabilistic algorithms have been proposed which incorporate prior information on the mechanics of plume dispersion with locally sampled sensor measurements. In addition to algorithms, the robot platforms themselves have evolved over time, with unmanned aerial vehicles (UAVs) now being utilized in much of the current research. The three dimensional (3D) navigation capabilities allow for the whole plume

phenomenon to be exploited and captured, inspiring a range of 3D sampling strategies and algorithms. Although UAVs may offer a better insight into the distribution of gas within the whole search volume, they introduce additional challenges that are not as prevalent for unmanned ground vehicles (UGVs), something that will be discussed further in this review paper.

One of the most common tasks undertaken by gas sensing robots is the production of gas distribution maps, which can be used to visualize the distribution of a chemical over an area of interest. Not only is this useful in determining the locations of gas leaks, but also the regions where a high concentration of gas has began to form. Another important topic in the subject of mobile robot gas sensing is the development of robot-mounted open sampling systems (OSS) which can be used to detect, discriminate, and quantify various gases. In situations where multiple different kinds of gas sources are present, such a device allows for each gas to be classified and independently represented within the gas distribution map. Referred to as an electronic nose (E-nose), this paper will provide a more detailed explanation of this topic in comparison to most review papers, to give more insight into the challenges faced by chemical sensing in uncontrolled environments.

There are many review papers on the subject of gas source localization and mapping with mobile robots. One of the most comprehensive review papers is presented in Lilienthal et al. (2006) which covers much of the early work on the subject. More recent reviews presented in Chen and Huang (2019) and Ishida et al. (2012) provide a summary of common biologically inspired algorithms used for gas source localization and an introduction to probabilistic source localization. However, much of the recent work on probabilistic source localization and mapping is not discussed, which will be a focus of this review. Furthermore, the challenges faced when using UAVs is not touched upon, which is a future trend for the field. Therefore, this review aims to provide a thorough overview of recent research and challenges. The publications included in this review paper were identified through searching relevant keywords in search engines such as "ProQuest" and "Google Scholar," and through general web searching. The total structure of the paper can be summarized by the following topics: gas sensing hardware and electronic noses, robotic platforms, gas source localization algorithms for both single robot and multirobot teams, and gas distribution mapping with mobile robots.

2 | GAS SENSING HARDWARE

Many different types of sensors have been used on mobile robots to detect gases and pollution. The types of sensors are normally chosen based on five properties: size, sensitivity, selectivity, response time, and reliability (Korotcenkov, 2007). Some sensors are quite large in size, which limits the number that can be used on a robotic platform. This is especially problematic if the sensor can only detect one type of gas, which in turn limits the usefulness of the robot.

As there is a focus to develop gas sensing robots for use in uncontrolled environments, the gas sensors used need to be sensitive enough to detect airborne chemicals whose source may be located some distance away. This is especially important in outdoor applications where gases are predominantly dispersed by wind rather than diffusion. The turbulent airflow caused by the wind creates a chemical plume, which becomes more diluted over time as it mixes with particles of clean air (Roberts & Webster, 2002). Not only does it become weaker, but it also begins to possess a patchy gradient that rapidly fluctuates in concentration. In such situations, some chemical sensors struggle to react to the rapidly changing odor plume. In addition to this, real-world scenarios typically feature multiple gas sources producing a gas mixture. Depending on the selectivity of the sensor, it may respond to multitude of gases, making determining the chemical composition of the air difficult. For this reason, some gas sensing robots use an E-nose, a device that contains an array of partially selective sensors allowing for gas discrimination algorithms to be applied to the sensor responses. This section will discuss the most commonly used sensors when gas sensing with mobile robots and explain the limitations that need to be considered when using them.

2.1 | Metal oxide (MOX) gas sensors

MOX sensors, alternatively referred to as semiconductor metal oxide (SMO) sensors, are one of the most commonly used chemical sensors in robot applications. This is mainly due to their small size, low cost, and high sensitivity. There are also many different MOX sensors available for detecting a wide variety of gases, making them an ideal choice for E-nose sensor arrays. For a stable and accurate output, MOX sensors require an initial warm up period to allow the sensor to achieve chemical equilibrium with the atmosphere (Peterson et al., 2017). Although some sensors require a warm up period of roughly 24 h for a completely stable output (Mokrani et al., 2019), for mobile robot applications where a stable sensor output signal is unlikely, the inaccuracies introduced from a shorter warm up period are effectively negligible.

It is common for low-cost MOX sensors experience signal drift, a form of permanent error that can limit their lifespan in long-term applications. Signal drift occurs due to the effects of sensor ageing, which in turn leads to a drift in the sensor's sensitivity over time (Maag et al., 2018). External factors such as temperature and humidity can also cause a temporary error in sensor readings, something that can be reduced by implementing calibration techniques (discussed later in Section 2.5.3). MOX sensors characteristically have poor selectivity. The MQ-2 MOX sensor can react to a multitude of different chemicals (Mokrani et al., 2019), which is beneficial when multiple chemicals are to be detected, but makes discrimination more challenging. Another problem that needs to be considered is their slow recovery time after a target gas has been removed (Figure 1). The slow recovery means MOX sensors typically act as low-pass filters (Burgues & Marco, 2019), therefore measurements often contain contributions from previous elevated levels of concentration.

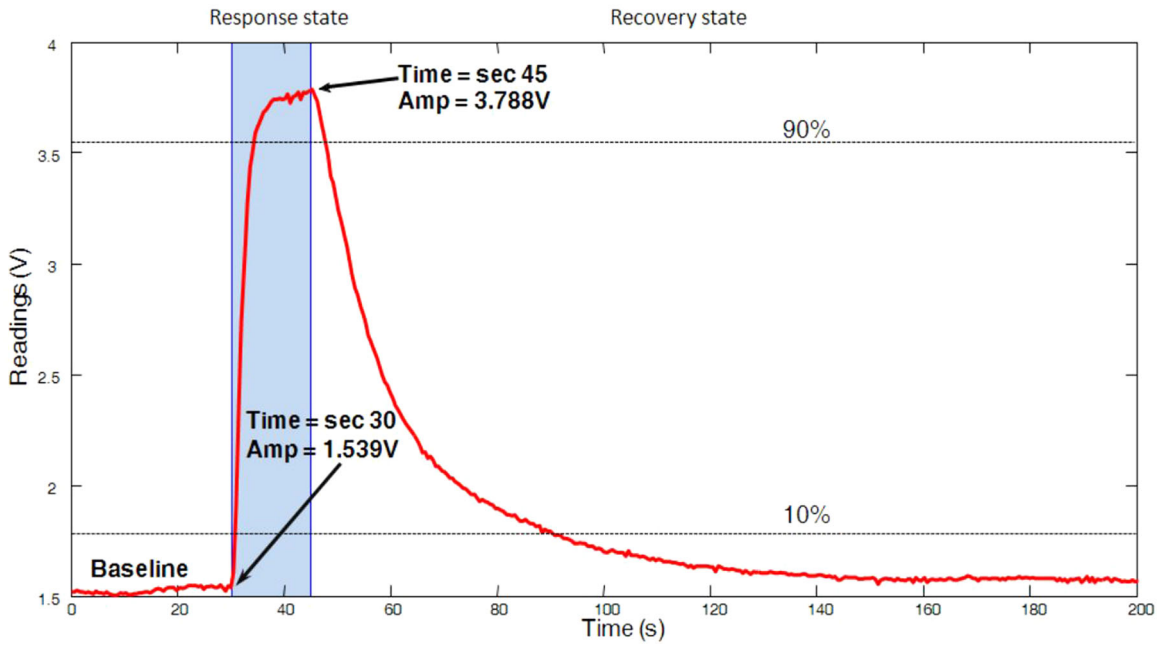

FIGURE 1 Typical MOX sensor response to target gas. Reproduced from Gonzalez-Jimenez et al. (2011). Licensed under CC BY 3.0 (https://creativecommons.org/licenses/by/3.0/). [Color figure can be viewed at wileyonlinelibrary.com]

2.2 | Particulate matter (PM) sensors

PM sensors are used to detect small airborne particles, they are commonly referred to as dust sensors. Although not a chemical sensor, they are extensively used in static monitoring stations to ensure that airborne pollution does not exceed legal requirements (Mooney et al., 2006). Lower-cost portable PM sensors known as optical particle counters (OPC) have shown to be a useful modality for mobile robots, with uses ranging from dust pollution mapping in industrial environments (Bennetts et al., 2016; Schaffernicht et al., 2017) to source localization (Chen et al., 2020).

Ambient air is pulled through the sensor by negative pressure generated by a fan. Within the sensor module, a light source illuminates the solid particles of dust in the air, which causes the light to become scattered. The scattered light is then measured by a photometer, allowing for the particle concentration to be calculated (Jovašević-Stojanović et al., 2017). PM is subdivided into different fractions based on the size of particles and where they can deposit within the human respiratory system, the primary fractions being PM10, PM2.5, and PM0.1 (Anderson et al., 2012). PM sensors are therefore generally categorized by the size of PM they can detect, with the most common being PM10 and PM2.5 sensors. The technology used within OPC sensors has given way for many compact and low-cost PM sensors to be brought to the market. Although the price of such sensors is low, it has been shown that they can provide accurate PM concentration data, comparable to the results obtained with gravimetric methods (Kelly et al., 2017).

OPC sensors do come with the drawback of being influenced by humidity. Laboratory experiments conducted by Jayaratne et al. (2018) found in the case of the PMS1003 OPC, the output remained stable until the relative humidity reached around 78% (Figure 2) at which point PM concentration began to be overestimated. There are several reasons for the error caused by humidity, the most common being the counting of fog droplets and the growth of particle size due to vapor condensation (Liu et al., 2019). The effect of humidity can be reduced by using calibration methods, such as by using modified linear compensation models (Hojaiji et al., 2017), linear regression methods (Chen et al., 2018), and combinations of linear and nonlinear calibration methods (Lee et al., 2020).

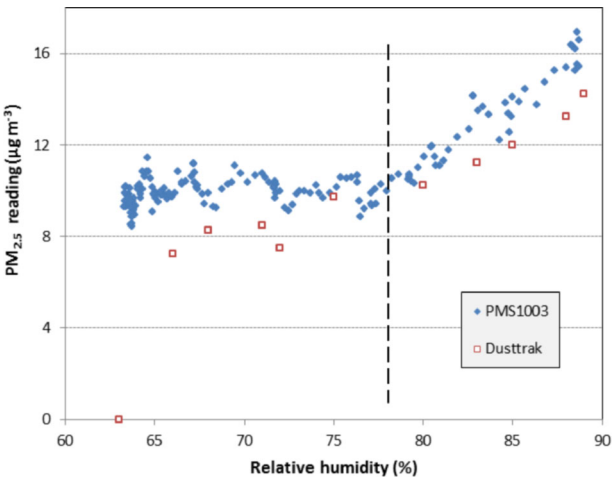

FIGURE 2 PM sensor drift due to relative humidity. PM, particulate matter. Reproduced from Jayaratne et al. (2018). Licensed under CC BY 4.0 (https://creativecommons.org/licenses/by/4.0/). [Color figure can be viewed at wileyonlinelibrary.com]

2.3 | Tuneable diode laser absorption spectroscopy (TDLAS)

The use of TDLAS in gas sensing robot applications has been an emerging trend in recent times, due to the technique's ability to detect gas remotely. The sensors provide benefits for both UGVs, where large areas to be monitored without needing to physically travel to each location (Bennetts et al., 2013), and for UAVs, where chemicals can be detected in the air column between the UAV and the ground (Emran et al., 2017). The technique is based on the intensity of monochromatic light passing through a uniform absorbing gas, given by Beer's Law (Goldenstein et al., 2017). Many gases absorb IR light and have peak absorption at specific wavelengths. If a laser emitting wavelength of IR light within the range of the peak absorption passes through a plume of gas, there will be a noticeable decrease in the detected light. Various hydrocarbons including methane (CH_4), propane (C_3H_8), ethylene (C_2H_4), ethane (C_2H_6), propene (C_3H_6), acetylene (C_2H_2), all have strong absorption features in the 1–4 μm range of infrared (IR) light (Dong et al., 2016).

There are many TDLAS sensors available in the market, the Sewerin remote methane leak detector (RMLD) is an example which is often used on robotic platforms due to its portable size and high sensitivity. However, such commercially available sensors are very expensive when compared to other kinds of gas sensors. Examples of purpose-built TDLAS sensors created by the authors have been used in mobile robot applications (Anderson et al., 2006, 2014; Chen et al., 2012). When designing purpose-built TDLAS sensors, optics are required for emitting the IR light along with detecting it when it has been reflected. In the case of Anderson et al. (2014), a telescope was used to collect and intensify the reflected light onto the photo-detector. It was found that large telescopes would shake in the wind and cause the reflected signal to be noisy. For cases where long sensing ranges are not required, compact lenses can be used, such as plastic Fresnel lenses (van Well et al., 2005).

When sensing over extreme ranges, stationary reflective targets can be used to increase the amount of light that is reflected back at the TDLAS receiver. For this technique to work effectively, the TLDAS sensor must be targeted directly at the reflector. An approach presented by Chen et al. (2012) achieved this by mounting a green spherical target above the reflector. A camera attached to the TDLAS sensor would then detect the green target and then center it within the picture frame, targeting the TDLAS at the reflector in the process.

2.4 | Photoionization detectors (PID)

PID are a type of chemical sensor similar in size to a standard MOX sensor. They are used to measure and quantify volatile organic compounds (VOCs) and work by breaking down the target gas into positive and negative ions through ionizing the sample with ultraviolet light (Patel et al., 2009). The resulting ions produce an electric current proportional to the output signal, measured with electrodes within the sensor (Spinelle et al., 2017). PIDs have a high bandwidth and sensitivity, with examples such as the "miniPID" having a frequency response of 300 Hz (Bailey et al., 2005). Their high bandwidth makes them well suited to gas sensing mobile robot applications, however, there are far less examples of their use when compared to MOX sensors due to their lack of selectivity and relatively high price point. For these reasons, PID sensors are often alternatively used to provide ground truth reference measurements to validate MOX sensor signal processing techniques, used to improve response times and performance (Burgues & Marco, 2019; Burgués et al., 2019). Similar to MOX sensors, PID sensors can experience signal drift in the presence of humidity, caused by an induced leakage current between the electrodes within the sensor. However, when the electrodes are clean, these effects are only seen at levels of relative humidity near to 100%, and so can be reduced through regular preventative cleaning (Butterfield, 2021).

2.5 | E-noses

MOX sensors are the most commonly used chemical sensor for gas sensing robots, due to their high sensitivity, low cost, and small size. However, their lack of selectivity means that in cases where multiple gases are present, it would be impossible to identify the type of gas being detected if only a single sensor was used. Knowing the identity of a detected chemical is especially important for chemical distribution mapping, as distribution maps can be produced for separate chemicals if multiple sources are present (Hernandez Bennetts et al., 2014).

2.5.1 | E-nose configuration

The general configuration of an E-nose includes a gas sensor chamber to house the array of chemical sensors and a pump to pull air through the chamber (Figure 3). An airflow feedback system can be used to monitor the volume of air being pulled through the chamber to ensure that the amount of air being sampled remains constant regardless of changing external conditions. In some cases, an air filter is situated at the inlet of the E-nose to reduce the amount of PM that would build up on the chemical sensors over time. An example that demonstrates these features is presented in Xing et al. (2017), where stop valves are also included to immediately cut off any air from being sampled if the ambient temperature exceeds safe levels. This was inspired from the E-nose developed in Wei et al. (2016), which was improved by including a larger array of MOX sensors along with enhanced signal processing capabilities.

2.5.2 | Sensor array response in open sampling systems

Chemical sensors used in closed sampling systems (CSS) will usually output a response that features three phases: response, steady state,

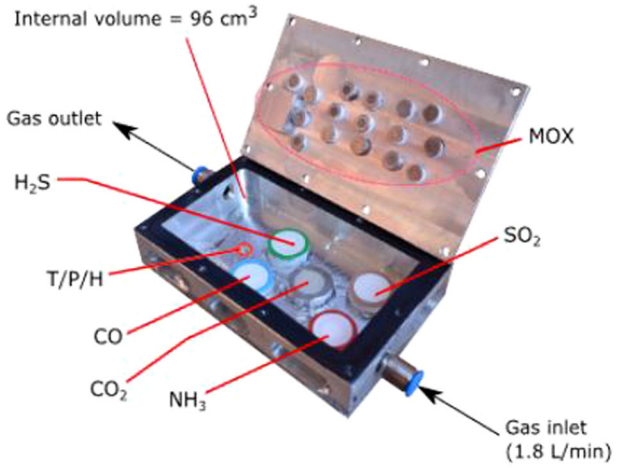

FIGURE 3 The RHINOS E-nose chamber containing an array of chemical sensors. Reproduced from Burgués et al. (2021). Licensed under CC BY 4.0 (https://creativecommons.org/licenses/by/4.0/). [Color figure can be viewed at wileyonlinelibrary.com]

and recovery. In the case of CSS, the sensor readings can be taken from the steady state region of the sensor response where the outputted sensor value is stable. In OSS such as E-noses, steady state is often never reached due to fluctuations in concentration caused by turbulence and advection of the airflow (Trincavelli, 2011). The fluctuations in concentration are often faster than the MOX sensors can respond to, producing a signal that features a number of peaks in comparison to a clear step change. As no steady state region is available to sample from, various preprocessing techniques must be used to extract useful information from the sensor response.

2.5.3 | Drift correction

As mentioned in Section 2.1, sensor drift is a source of error caused by the ageing of the sensor, although it is also temporarily caused by external factors like changes in relative humidity and temperature (Abdullah et al., 2020). Therefore, it is important to correct for sensor drift before utilizing the sensor response for gas quantification purposes. One of the most common methods of drift compensation is baseline manipulation which uses the initial value of the transient response known as the baseline to correct the final output. There are three baseline manipulation techniques which are most commonly used: differential, relative, and fractional (Gutierrez-Osuna & Nagle, 1999).

1. Differential: Baseline value for each sensor is subtracted from the output value:

$$S(t) = G(t) - G(0). \tag{1}$$

2. Relative: Output value is divided by baseline value which can help correct for multiplicative drift:

$$S(t) = \frac{G(t)}{G(0)}. \tag{2}$$

3. Fractional: Baseline value is subtracted from sensor response and divided by baseline value:

$$S(t) = \frac{G(t) - G(0)}{G(0)}, \tag{3}$$

where $S(t)$ is the corrected sensor output and $G(t)$, $G(0)$ is the sensor conductance and baseline conductance, respectively. Although baseline manipulation is simple, it does not always provide good results in realistic situations. Equations (1) and (2) often fail when used to normalize the sensor response as drift is generally not additive nor multiplicative (Di Carlo & Falasconi, 2012). Research conducted by Ahmadou et al. (2017) found that the fractional baseline manipulation shown in Equation (3) did not improve gas discrimination, mainly due to the variation of $G(0)$ from temporary drift caused by gas sampled in previous measurements. To obtain a more notable drift compensation, the equation was modified to use the final value of the transient response (end of recovery phase) instead of the initial baseline value. This was found to give a clear improvement in gas discrimination in cases where sensors cannot be purged with clean air:

$$S(t) = \frac{G(t) - G(\text{final})}{G(\text{final})}. \tag{4}$$

2.5.4 | Feature extraction and gas classification

Feature extraction is the process of extracting useful information from the transient response of the sensor array in order for pattern recognition algorithms to classify the sampled chemical. Fourier transform analysis is a technique which is synonymous with characterizing rapidly changing signals, and in the case of Nimsuk (2014), short-time Fourier transform (STFT) was used to extract information from the response of four MOX sensors. STFT is a Fourier-based method for determining the sinusoidal frequency and phase information of local sections of a signal through using a "window function" which is slid along the time axis. Following the frequency analysis, stepwise discriminant analysis was employed which used Wilks' lambda (Dillon & Goldstein, 1984) to select components that contributed the most to gas classification.

Another method of feature extraction for an array of MOX sensors was presented in Zhang et al. (2009), which instead focused on extracting information from the decay or recovery section of the MOX transient response allowing for fast pattern recognition. This was inspired from results gained in their previous research (Zhang et al., 2008), which found that the shape of the recovery curves did not change much when chemical sample time was varied, even though steady state was not reached. Gas classification was achieved by extracting two time parameters from the response curves:

recognition time (time taken to respond to the chemical), and response-recovery time (time taken to respond and recover). These values were initially extracted for each MOX sensor by using samples of known gas and then compiled into a learning data set, allowing for discriminant function analysis (DFA) to be used for classification. This was found to classify unknown samples with an accuracy of 100%.

A similar approach was taken in Mishra et al. (2013) where the response/recovery curves of the sensor responses were used to classify gases. First, training data was collected for four different chemicals at different concentrations, where data was extracted with a graph extracting tool. Having plotted the resulting data on a 3D scatter plot, it could be seen that the raw data overlapped in its current form. To obtain less overlapped clusters, data was transformed using an average slope multiplication (ASM) method, which is based on multiplying the sensor response/recovery data by its respective average slope. This method was used as it could be seen that the sensor response curves had different slopes for a particular concentration band of a particular chemical. Following ASM, clear clusters of data were apparent, and so neural classifiers were applied to classify the transformed data. By using a combination of principal component analysis (PCA) to reduce dimensionality and a gradient descent with back propagation (GDMBP) neural network as a classifier, 100% classification accuracy was achieved for the four chemicals.

Using previously acquired learning data sets allows for many discrimination algorithms to be used, although in OSS their use can be limited by the presence of unknown interferents. Creating a learning data set can also be time-consuming and expensive, which has led to the development of unsupervised gas discrimination techniques. Another problem to consider is that the data is often distributed in random shapes, and classical unsupervised learning methods like K-means cannot detect nonspherical shapes (Tseng & Yang, 2000). To tackle these problems, an unsupervised gas discrimination approach was proposed in Fan et al. (2016) which clustered the density peaks of the transient responses of a MOX sensor array. Based on the algorithm originally presented in Rodriguez and Laio (2014), the algorithm uses an adaptive estimation, meaning that when the density of clusters differs, the peak local density of a point will still be close. The improved algorithm works on the assumption that the clusters are surrounded by neighbors that feature a lower local density ρ and a minimum distance to higher density clusters δ. Practical experiments conducted using a mobile robot fitted with an array of five MOX sensors showed that the algorithm was able to classify 95% of observations, for a room that contained two different chemical sources. It was noted however that some misclassifications occurred at low concentration levels.

Misclassifications are a common problem with density-based classifiers, as they can make overly confident predictions in densely populated regions, such as at values of low concentration. A different approach was proposed in Bennetts et al. (2014) which takes advantage of the correlation between class separability and concentration level. At low concentration levels, there is a clear overlapping between classes which can make discrimination difficult, whereas at high concentrations there is a more pronounced difference. The proposed algorithm assigns higher posteriors in regions where there is large separability and low posteriors to regions of overlapping. In addition, a rejection posterior is learned such that a high rejection signifies the sensing of clean air. When testing the proposed algorithm on data gathered by a mobile robot in indoor and outdoor environments, the success rate for classification was found to always be above 93%. Higher success rates could be achieved by using a more complex model, however, the potential improvements were not all that significant and risked over-fitting the model.

2.5.5 | Gas quantification with an array of MOX sensors

Both gas source localization, and distribution mapping algorithms often require spatially sampled measurements of the gas concentration. In the case of OSS that utilize MOX sensors, it can be particularly difficult to quantify the detected chemical. This is again caused by the problem of never reaching a steady state transient response phase due to the MOX sensor's slow response to the rapidly changing turbulent chemical concentration found in natural environments. Similar to gas classification algorithms, gas quantification algorithms often select features from the sensor response and cluster them to find their most likely concentration values.

Following their success in developing a gas discrimination algorithm using ASM, Mishra et al. (2013) proposed using ASM to quantify chemical concentration (Mishra et al., 2013). Again, ASM was used to separate sensor response/recovery data in order for GDMBP to classify the data with a specific quantity. Training data was supplied using the response/recovery data gathered for four concentration bands of four different gases. When using a back propagation algorithm, the concentration of gas can be estimated regardless of how long the sensor is exposed to chemical, as the slope of the transient phase remains the same.

The K-nearest neighbor (kNN) classification algorithm has also been used to estimate the concentration of chemicals using the transient response of MOX sensors. An example of this can be seen in Rehman and Bermak (2018) where kNN was combined with a feature extraction method to classify and quantify six different chemicals using an array of 16 MOX sensors. kNN is an example of a non-parametric classifier which can be used for gas classification along with concentration estimation. In the case of concentration estimation, different concentration values are assumed as different classes, where concentration values are compared with that of a training data set.

Rather than giving a single prediction value for the chemical concentration, chemical quantification can be represented as a probabilistic problem by estimating the gas concentration using a switching linear dynamical system (SLDS) model (Di Lello et al., 2014). The technique works through learning the parameters of a first-order linear dynamical system (LDS) which could be fitted to the rise and decay phase of the sensor's response. Once the LDS parameters are

known, they can be used to compute the gas concentration via inference in the SLDS model. This probabilistic approach takes into account the uncertainties that arise from the error in sensor measurements and modeling errors, providing confidence measures for the estimated variables. It was found that the estimated chemical concentration values were comparable to the results from a PID sensor, providing a means to gain accurate sensor measurements in the absence of steady-state sensor outputs.

Alternatively, a data-driven approach to probabilistic chemical quantification is possible. Gaussian process regression (GPR) is a machine learning technique which aims to learn a function that fits noisy training data with a given confidence. In Monroy et al. (2013), GPR was used to estimate the detected chemical concentration using training data from a set of baseline corrected sensor readings sampled by an array of MOX sensors. GPR uses a covariance function to smooth the data, which in this case was chosen to be a squared exponential covariance function. The length hyperparameter used in the covariance function determines how correlated the data is, including how much effect distant data points have on estimated values. The hyperparametrs used in GPR need to be suitably chosen, which can be done through maximizing the marginal likelihood function for the vector of training concentration values given the sensor array measurements and vector of hyperparameters. To further reduce computational complexity, automatic relevance determination (ARD) was applied during the training phase of the GP which reduces training data through selecting the sensors providing the most relevant contributions. By comparing the results from the GPR algorithm with ground truth concentration data from a PID sensor, it was found that the use of an array of sensors provided better prediction quality when compared to the results for a single sensor.

3 | MOBILE ROBOT PLATFORMS

This survey paper will focus on the two most common types of mobile robot platforms used for gas source localization and mapping: UGVs, and UAVs. The two types of robots both come with benefits and limitations which should be considered when determining which platform would be better suited to a particular gas source localization or mapping application.

3.1 | Unmanned ground vehicles

Much of the work on gas source localization and mapping has been completed with UGVs. Small differential drive robots are often used to quickly test algorithms in small-scale indoor experiments (Hutchinson et al., 2019; Lu, 2013). Larger UGV platforms capable of operation in both indoor and outdoor environments are often used for field experiments (Bennetts et al., 2012; Wandel et al., 2001). Their larger size and battery life allows for a range of sensors to be equipped to the platform (Figure 4), including LiDAR for simultaneous localization and mapping (SLAM) and obstacle avoidance, ultrasonic anemometers for wind velocity measurements, pumped E-noses containing arrays of chemical sensors, large TDLAS sensors mounted on pan-tilt units, and global positioning systems (GPS) for outdoor localization.

UGVs allow for greater on-board resources available for online computation of complex algorithms, and the slow movement speed of UGVs and their ability to stop to take measurements allows for limited disruption to the chemical plume. UGVs are however hindered by difficult terrain and can only operate in two dimensions (2D), meaning that even with the use of multiple E-noses at different heights (Reggente & Lilienthal, 2009), only a limited portion of the plume can be detected from the ground, something that may be problematic for locating sources in high positions, or detecting lighter than air gases at distances further away from their source. In general, UGVs are better suited to applications which require a denser coverage of gas concentration measurements collected over a long period of time. Some of which include locating and mapping the distribution of methane at landfill sites (Hernandez Bennetts et al., 2012), detecting chemicals in underground mines (Kim & Choi, 2021; Martinez et al., 2020), gas pipeline leakage detection (Kroll et al., 2009), and gas source localization of near ground sources.

3.2 | Unmanned aerial vehicles

The use of UAVs for gas sensing applications is a recent direction for the field and comes with a whole new set of challenges. Although there have been examples of gas sensing using fixed-wing UAVs (Nathan et al., 2015), rotary-wing drones are the most commonly used UAV platform. This comes from the benefits that arise from their superior maneuverability, ability to stop and hover in a fixed position to take gas concentration measurements, and slower flight speeds which are more suited to slow responding chemical sensors when sampling on the move. Small UAVs often used in gas sensing applications can be categorized into three sizes: mini drones that weigh between 5 and 2 kg, microdrones that weigh between 2 kg and 200 g, and nano drones which have a weight of less than 200 g (Brooke-Holland, 2012). For the purpose of simplicity, this paper will refer to both micro and mini drones as mini drones, as their performance and limitations are typically similar.

Mini drones allow for a greater array of sensors to be equipped to the drone due to their larger payload and battery capacities, along with their overall longer flight times. They will however still experience a linearly decreasing flight time with increasing payload weight (Zhang et al., 2021), further reduced from the additional power drain of the sensors themselves. These constraints are even more restrictive for nano drones, with examples such as the "Crazyflie" (Figure 5a), a 10×10 cm nano drone used in various works (Castro et al., 2018; Duisterhof et al., 2021; Ercolani et al., 2022; Neumann et al., 2019), only having a maximum payload

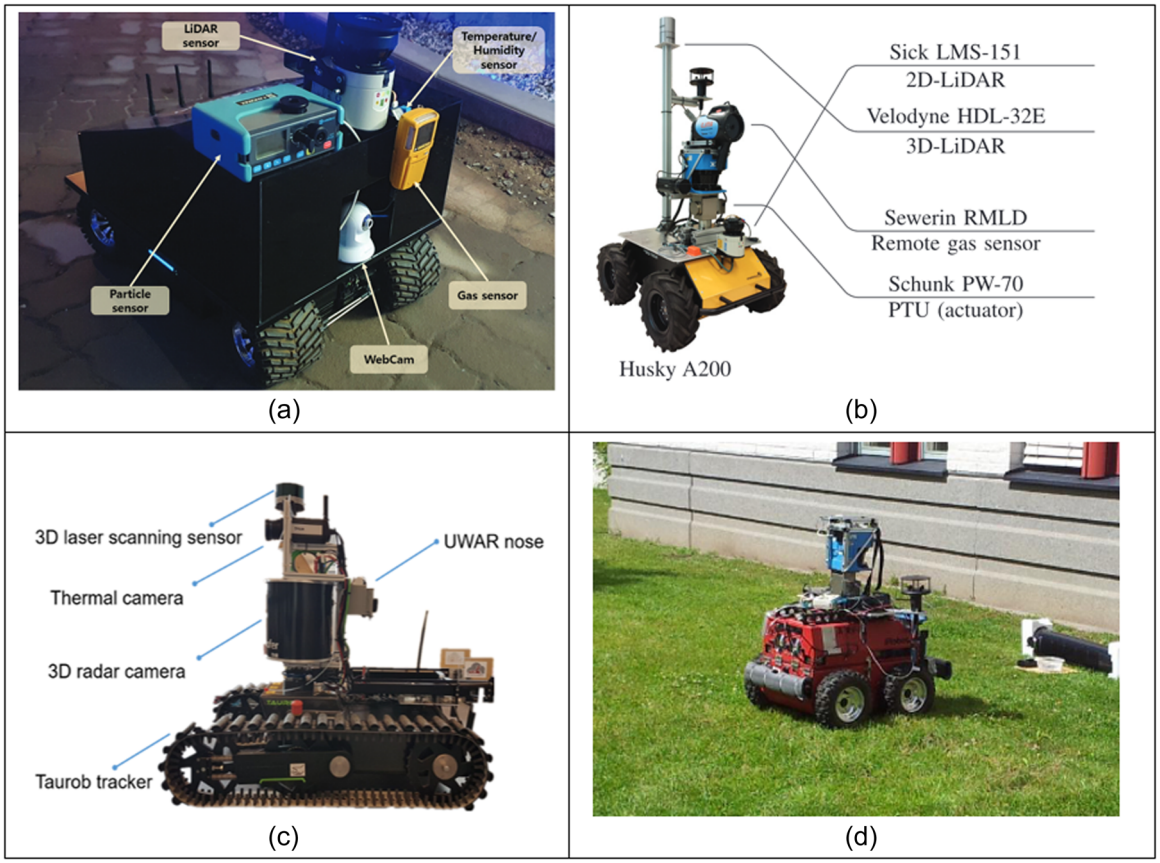

FIGURE 4 Examples of UGVs used for gas sensing applications. (a) ERP-42 robot for environmental monitoring in underground mines. Reproduced from Kim and Choi (2021). (b) ARMEx robot based on the Husky A200 platform for remote methane detection and mapping with TDLAS sensor. Reproduced from Arain et al. (2021). (c) SmokeBot for gas distribution mapping in emergency scenarios. Reproduced from Fan et al. (2019). (d) ATRV-JR robot fitted with E-nose for gas distribution mapping of multiple chemical compounds. Reproduced from Hernandez Bennetts et al. (2014). (a)–(c) licensed under CC BY 4.0 (https://creativecommons.org/licenses/by/4.0/). (d) licensed under CC BY 3.0 (https://creativecommons.org/licenses/by/3.0/). [Color figure can be viewed at wileyonlinelibrary.com]

capacity of 15 g and flight time of 7 min (Giernacki et al., 2017). Nano drones do however provide some benefits. Their compact size means that the effects of the turbulence caused by their propellers on the plume structure is reduced, and operation in indoor and cluttered environments which might otherwise be inaccessible for larger drones or UGVs is possible. The use of UAVs for gas sensing applications poses many unique challenges, and therefore will be discussed in greater detail in this section.

3.2.1 | Chemical sensor payload

The problem of propeller-induced turbulence, alternatively referred to in literature as "wake," is a key problem that must be considered for both mini and nano drones. Villa et al. (2016) found that gas concentration readings detected with a chemical sensor-equipped mini drone decreased dramatically once the propellers were turned on, suggesting that the wake dilutes the gas concentration with clean air. To avoid this problem, they mounted chemical sensors on a boom that extended beyond the wake region caused by the propellers. Small TDLAS sensors can instead be used to avoid this problem (Figure 5b), as their beam can detect chemicals far outside of the region of wake (Iwaszenko et al., 2021; Neumann et al., 2018). However, TDLAS sensors are heavy and expensive, requiring larger UAVs to carry them increasing the overall platform price. Alternatively, a ventilated E-nose can be used where air is drawn in through a protruding tube with the inlet located outside of the region of wake (Figure 5c). This way, the weight of the E-nose is centered on the UAV, and more flexibility is given in terms of inlet position and type.

Rather than using a long E-nose inlet pipe which could cause flight stability problems, Neumann et al. (2012) mounted chemical sensors within a carbon fiber tube, where air was drawn through it using the suction effect of one of the propellers. This semi-active transport approach was found as a good compromise between directly mounting the sensors in a passive approach and using a long boom. Such approaches may still be less effective at closer distances to point sources, where the downwash could greatly affect the gas distribution. To avoid this, long sampling tubes can be suspended from the UAV, placing the inlet far outside of the region of wake. A 10 m suspended sampling tube was used by Burgués et al. (2021) for

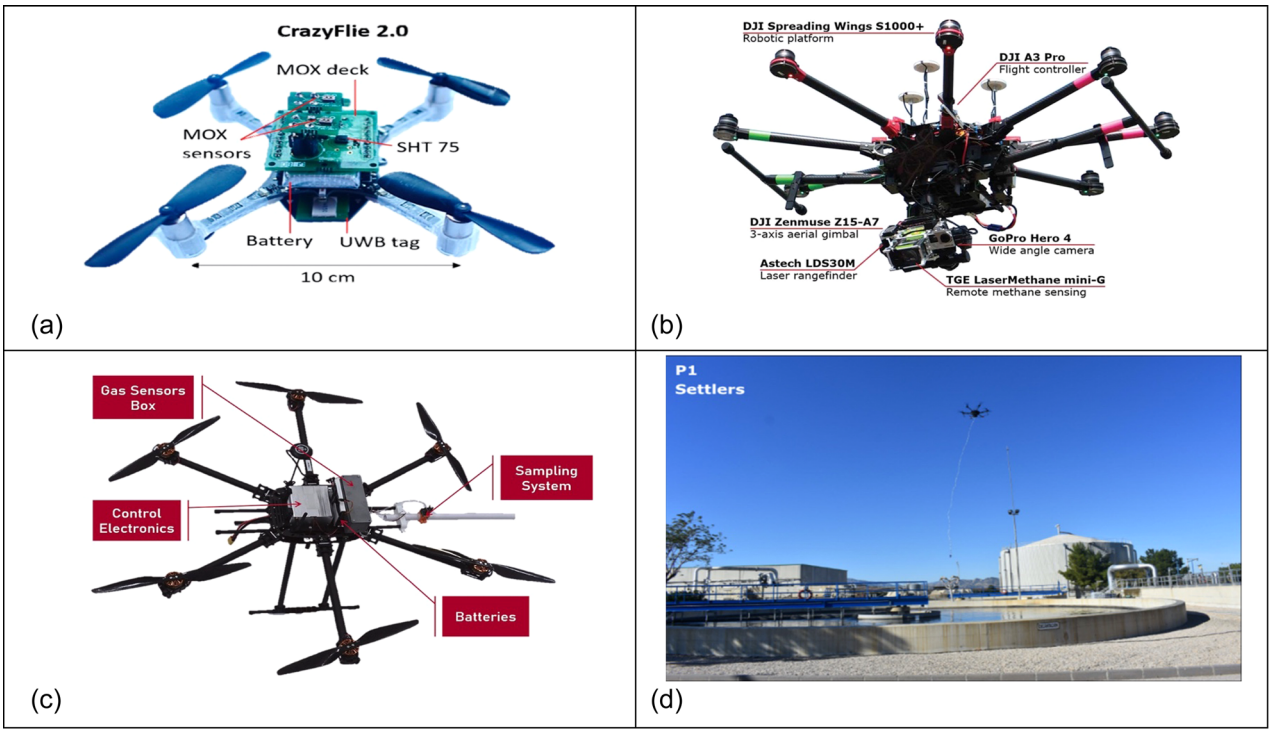

FIGURE 5 Examples of UAVs used for gas sensing applications. (a) Crazyflie 2.0 nano drone equipped with MOX sensor, adapted from Burgués et al. (2019). (b) DJI Spreading Wings S1000 mini drone equipped with TDLAS sensor. Reproduced from Neumann et al. (2019). (c) Hexacopter mini drone equipped with E-nose using protruding inlet tube. Reproduced from Arroyo et al. (2022) with permission from Elsevier. (d) DJI Matrice 600 Pro equipped E-nose using suspended 10 m sampling tube, adapted from Burgués et al. (2021). (a,b,d) licensed under CC BY 4.0 (https://creativecommons.org/licenses/by/4.0/). [Color figure can be viewed at wileyonlinelibrary.com]

gas distribution mapping of a water treatment plant (Figure 5d). Although accurate point measurements could be achieved under ideal environmental conditions, the tube would be blown from its vertical position by wind and would not be usable in cluttered environments where the tube could become tangled with obstacles during navigation. Ventilated approaches are still not applicable to nano drones due to their limited payload and battery capacities.

To explore the effects of wake on chemical sensor placements, Do et al. (2020) used particle image velocimetry (PIV) to study the air velocity field around a hovering mini drone. They found four potential locations where airflow was most stable: in the center on top of the drone (top), in the center below the drone (bottom), on the side of the drone's center (middle), and in a specific region below the drone's propeller (rotor). The middle position was found to provide the best performance in terms of detected chemical intensity and response time, followed by bottom, top, and rotor, respectively. A similar conclusion on sensor position was drawn following CFD simulations in Kuantama et al. (2019). For a chemical sensor located forward from the drone's center, they suggested that surrounding gas would be pulled through the sensor before being directed downward by the suction from the propellers. This was validated by field tests which found for a hovering drone the detected gas concentration remained farily stable for the offset position, but was reduced significantly for the central position. For nano drones, it may be difficult to mount a forward middle position chemical sensor due to the limited space available, which would suggest that a bottom-mounted central position may provide the best compromise. This conclusion was supported by experimental results achieved in Ercolani and Martinoli (2020), which found that a nano drone bottom-mounted chemical sensor produced lower variability and higher success rates when compared to a top-mounted configuration in gas source localization trials.

3.2.2 | Localization and obstacle avoidance

The sensors that can be equipped to mini drones are typically similar to those that are used on UGVs. These include LiDAR sensors (Bachrach et al., 2011; Winkvist et al., 2013), or cameras (Latif & Saddik, 2019; Rhodes et al., 2022; Yang et al., 2018), allowing for SLAM algorithms to be used for obstacle avoidance and localization. SLAM algorithms are computationally expensive (Bodin et al., 2018), often requiring memory and processing capabilities far exceeding that offered by nano drones. Although offline computation may provide a solution, the weight and power requirements of such sensors are also in excess of the limits imposed by nano drones. Instead, mapless navigation solutions are required that make use of basic obstacle avoidance sensors. A common technique is to mount laser rangers onboard the nano drone (Duisterhof et al., 2019), allowing for simple obstacle avoidance strategies such as the bug

algorithm to be applied (Duisterhof et al., 2021). Still, examples of successful obstacle avoidance in more complex environments are few, which currently limits their autonomous navigation capabilities in real-world scenarios.

Localization can typically be achieved by UAVs in outdoor environments by using GPS (Croizé et al., 2015; Santana et al., 2015). For indoor and other GPS-denied environments, external localization systems are often used, with the primary options being motion capture systems, and ultra-wide band (UWB) systems (Masiero et al., 2019). Motion capture systems use an array of cameras to offer very precise localization and often serve as ground truth for performance evaluation (Yang & Yang, 2021), however, they are significantly more expensive than UWB systems and require a direct line of sight between the cameras and drone. UWB systems are relatively inexpensive and offer localization accuracy of around 10 mm (Gentner & Ulmschneider, 2017). The UWB system consists of an array of anchor nodes distributed around the area of operation, and a tag node located on the UAV. To further improve localization accuracy, many works use an extended Kalman filter to fuse UWB and internal measurement unit (IMU) data (Ercolani & Martinoli, 2020; Li et al., 2018; Nguyen et al., 2016). The positional error increases at greater distances from the anchors (Puschita et al., 2020), and so a sensor fusion approach can provide better overall performance and reduced error.

3.2.3 | UAV applications

As long as suitable modifications have been made to limit the effects of propeller-induced turbulence on chemical sensor readings, the longer flight times offered by mini drones allow for more conventional gas source localization and mapping algorithms to be used, albeit with shorter sampling times (Hutchinson et al., 2019; Neumann, 2013; Neumann et al., 2013, 2012). Mini drones are suited to applications which require fewer gas concentration measurements to be collected quickly over very large areas, or sampling in environments and locations which would be out of reach for UGVs. Examples include, measuring volcanic gas emissions (Arellano et al., 2019), air pollution monitoring over areas of open cast mining (Ren et al., 2019), monitoring the emissions from maritime vessels (Yuan et al., 2020), locating and quantifying hazardous chemical releases (Hutchinson et al., 2019), and localizing and mapping emission hotspots from civil waste treatment facilities (Burgués et al., 2021; Fjelsted et al., 2019).

For nano drones, stopping to hover and gather time-averaged gas concentration measurements would quickly deplete their limited battery resources, only allowing for a small sample of measurements to be taken. A "butterfly" style strategy can overcome this by landing and stopping to collect measurements (Rossi & Brunelli, 2017), but this does not allow the drone to sample the whole 3D plume phenomenon and limits the drone to measuring ground-level gas concentration. Instead, it may be beneficial to collect measurements in motion, at the expense of measurement accuracy. MOX sensors are most used chemical sensor in UAV applications, with ultra-small microelectromechanical systems (MEMS) based MOX sensors being especially applicable (Castro et al., 2018; Duisterhof et al., 2021; Rossi et al., 2014). Previously, Lilienthal et al. (2001) were able to locate a chemical source using MOX sensor measurements taken with a UGV in motion, suggesting that such an approach may be possible. Similarly, Bing et al. (2015) were able to locate a chemical source using MOX sensor measurements taken in motion with a UAV. They noted that the MOX sensor was only able to detect gas in a few positions, with a greater number of sensor responses happening near the source. These findings have been leveraged in more recent works to localize gas sources using measurements taken in motion with nano drones (Burgués et al., 2019; Ercolani & Martinoli, 2020). Although a recent direction for the field with few examples of practical experiments in larger environments, such approaches would allow for rapid localization and mapping of gas, extremely beneficial for emergency or other time-sensitive situations.

4 | GAS SOURCE LOCALIZATION (GSL)

GSL is the task most often assigned to chemical sensing robots, in fact, most of the early research on the subject was focused solely on source localization. This makes sense, as traditionally animals like dogs have been used to locate chemicals using their superior sense of smell. However, animals can be unpredictable, they must be trained, and often the applications where they are can be dangerous for themselves and their human handlers. For these reasons, mobile robots were investigated as potential platforms to undertake such tasks.

4.1 | Bioinspired searching

Many early GSL algorithms were heavily influenced by source finding techniques that can be seen in nature. The *E. coli* inspired algorithm is a chemotaxis example which consists of making straight-line runs separated by random turns (Macedo et al., 2019; Russell et al., 2003). If the most recent concentration is higher than the last, the robot makes a small turn followed by a large straight-line run. If it decreases, then the runs become much shorter, and the turns become larger. This simple strategy only requires the previous concentration reading to be stored, and therefore has very little memory requirements (Dhariwal et al., 2004).

Most bioinspired algorithms use wind information alongside the sensor readings. Referred to as anemotaxis, common examples include the dung beetle inspired algorithm (Russell et al., 2003) and lobster-inspired algorithm (Grasso & Atema, 2002; Grasso et al., 1998; Maes et al., 1996), both of which are dependent on a consistent chemical gradient to achieve successful results. Their operation being similar to that of Braitenberg style chemotaxis which guide robots through moving in the direction of highest concentration (Lilienthal & Duckett, 2004; Mamduh et al., 2013; Takei et al., 2014). One of the

most popular anemotaxis example is that of the silkworm moth inspired algorithm (Kuwana et al., 1996; Rutkowski et al., 2004). Rather than directly following a concentration gradient, the robot surges up-wind whenever the chemical is detected. Once contact with the chemical is lost, the robot casts from left to right in a perpendicular direction to the wind in the hopes of encountering another chemical hit. Various adaptations of this technique have been presented over the years (Harvey et al., 2008; Hayes et al., 2002; Ishida et al., 2005; Lilienthal et al., 2003; Waphare et al., 2010; Zhou et al., 2015), which generally vary the method of casting used to re-encounter the plume. For more detailed explanations of common bioinspired algorithms, the reader is referred to the review paper by Chen and Huang (2019).

Generally, research has moved away from classical algorithms based on concentration gradient. The assumption of a smooth and consistent chemical gradient is not often valid in realistic environments due to turbulence (Chang et al., 2013), and the reliance on a laminar airflow in non-diffusion-dominated environments means that robots using such algorithms may fail to track the chemical plume. Research by Hernandez Bennetts et al. (2012) found that laminar airflow was not found in both indoor and outdoor environments, pointing toward why such algorithms might struggle to work reliably in such situations.

4.2 | Probabilistic algorithms

Probabilistic approaches to GSL exploit mathematical models of the gas dispersion process to estimate the most probable location of the chemical source. Rather than trying to directly follow the plume gradient as in the case of chemotaxis, sparse measurements are taken in regions which are likely to reduce the amount of uncertainty of the source location, which eventually converges to one location once uncertainty is low.

4.2.1 | Infotaxis

The Infotaxis algorithm proposed by Vergassola et al. (2007) was one of the first probabilistic GSL algorithms. The algorithm uses a probability distribution to express the estimated position of the source within a lattice environment. The function is constantly updated with time by solving a Bayesian inference problem to reconstruct the probabilistic map. An indication of a successful search is given by the Shannon's entropy of the probabilistic map, which goes to zero when the source is localized to one location. The decoding protocol relies on an atmospheric transport and dispersion model (ATD) which can express the chemical encounters as a function of distance from the source. Once the probability density function (PDF) has been assembled, the robot decides whether to explore the area or exploit the most likely position of the source by choosing the direction which locally maximizes the rate of information gained at each time step. The Shannon's entropy of the PDF decreases with acquired information, and so the robot chooses the direction which maximizes its reduction. This guides the robot to the source in a similar way to gradient following algorithms, as it is expected that information accumulates faster close to the chemical source. The calculation for the variation in entropy includes terms that give the robot exploitative and exploratory tendencies based on the potential gain of information.

As the Infotaxis algorithm relies on multiple environmental parameters, the effect of inaccurately modeling the environment on the performance of the algorithm has been simulated (Rodríguez et al., 2014, 2017). It was found that the algorithm remained effective as long as the parameters did not vary too far from their actual values, as over and underestimation led to a rapid decay in performance. Simulations have also suggested that Infotaxis may be robust in dealing with pulsing plume sources (Martin Moraud & Martinez, 2010), where short pauses between pulses would cause the robot to navigate mainly upwind, and long pauses would instead cause the robot to counterturn and explore in large spirals. These results suggest that the Infotaxis algorithm should be fairly robust when dealing with realistic situations, even when the ATD model used does not exactly represent the real plume dispersal. The performance of Infotaxis has been compared with that of the biologically inspired dung beetle algorithm where simulations were performed for a odor model which combined turbulent and molecular diffusion (Siqi et al., 2012). The performance of the dung beetle algorithm decreased dramatically when the initial distance from the source was increased, however the success of the Infotaxis algorithm remained very consistent and only reduced by a small amount.

Modified infotaxis

Various adaptations of the Infotaxis algorithm have been proposed, such as a modified algorithm which uses a TDLAS sensor to reduce the searching time (Dai et al., 2019). This version of Infotaxis was referred to as line integral infotaxis (LII) as the path that the laser traveled was broken into multiple segments. The discretized optical path could be considered as the readings from multiple robots, so that the associated probability of each could be applied to reduce exploration time.

In Ristic et al. (2016), some of the source parameters of the ATD model were estimated through a Bayesian framework using sequential Monte Carlo, alleviating the 2D grid-based implementation of the original Infotaxis. The work also compared three information-theoretic reward functions: Infotaxis, modified Infotaxis (removing the term which coincides with the source being located at a node within the lattice), and a special case of Rényi divergence: Bhattacharyya distance. The results of simulations and an experimental data set found little difference in performance between the three, however, the original Infotaxis reward function was found to be slightly worse, possibly due to its overall greater exploitative tendencies.

Using the probabilistic framework to estimate the source parameters, Hutchinson et al. (2018) proposed improving the Infotaxis algorithm further to use maximum entropy sampling

principles. Named "Entrotaxis," rather than moving to the direction that would minimize entropy of the posterior distribution, the searcher moves to the location where the least is known about the next sample, therefore decreasing the entropy of the predictive measurement distribution. Simulations found that although the success rate of the Infotaxis and Entrotaxis algorithms remained the same, Entrotaxis performed better in terms of mean search time by following a more efficient search path.

As mentioned in Section 2.2, PM is measured based on particle size. This means that when localizing a PM source using Infotaxis, a choice would need to be made on what size of particle the algorithm should use. Instead, Chen et al. (2020) adapted the algorithm by integrating the measurements for six different sizes of PM. Simulations compared three integration strategies along with a single modality approach which only used one particle size. The results showed that using measurements for the smallest particle size was found to give the best results in the single modality approach. Of the multimodal strategies, the best integration strategy was found to be a weighted map approach which weighted the sum of all the available maps, where the weight of each map was represented by the reciprocal of its entropy. Wind tunnel tests using a UGV found that the integrated approach was able to locate the source with higher accuracy than the single modality approach, however more iterations were required. It was noted that the algorithm degraded in performance when the parameters of the dispersion model were inaccurate, cementing the importance of having accurate localization when using any Infotaxis strategy.

4.2.2 | Source term estimation

The original Infotaxis by Vergassola et al. (2007) utilizes an Isotropic plume model to construct a PDF for the location of the source, where the model parameters were assumed before simulations being conducted. In later algorithms, both source location and emission rate were represented as a PDF and estimated through Bayesian inference and efficient sampling methods (Hutchinson et al., 2018; Ristic et al., 2016). Often, the majority of the source parameters are unknown to the searching agent, so it is beneficial to represent each of them as a PDF, and iteratively update them with new information. This process is known as source term estimation (STE).

Traditionally, STE was conducted using networks of static chemical sensors (Rao, 2007). However, the resolution of sensors within such a network is limited, and it is impractical to cover all regions of interest with sensors. A survey by Hutchinson et al. (2017) covers most of the topics associated with static and mobile sensor STE, including both optimization and Bayesian inference approaches, along with mobile sensor methods to plume boundary approximation. This section will review mobile robot STE methods for source localization only, with a focus on Bayesian approaches. Examples of more recent works, along with experiments conducted in real-world environments will be discussed in this section.

Bayesian inference of the source term

Bayesian inference approaches to STE provide a probabilistic estimate of the source parameters, in comparison to optimization-based solvers which converge to the best estimate of the true parameters (Jensen et al., 2019). This is more desired in situations where input variables and underlying models are uncertain, as the uncertainty can be captured within a PDF (Hutchinson et al., 2017). Assuming that a vector of parameters $\boldsymbol{m}$ represents the parameters of an ATD model, Bayes' theorem can be used to manipulate the PDFs of $\boldsymbol{m}$ along with prior information I and samples of concentration data D to provide a PDF which represents the belief of the true source parameters:

$$P(\boldsymbol{m}|D, I) = \frac{P(m|I)P(D|\boldsymbol{m}, I)}{P(D|I)}. \tag{5}$$

This allows for the uncertainty in the observational and model data to be accounted for and allows for the fact that many source configurations may be possible, however, some will be more probable than others (Keats et al., 2007). By conducting inference with each new measurement, the previous posterior PDF can be set as the new prior. Initially, it is often assumed that no prior information is available, and so the prior is set as a uniform distribution within the limits of each parameter. It is common for the normalization factor (the evidence term $P(D|I)$) to be neglected by using efficient sampling techniques, mitigating the need to calculate a multidimensional and complicated integral.

Commonly used sampling techniques include (but are not limited to): Markov chain Monte Carlo (MCMC) (Hutchinson et al., 2017; Rahbar & Martinoli, 2020; Rahbar et al., 2019a), and sequential Monte Carlo (SMC) (Hutchinson et al., 2018, 2019). Metropolis-Hastings is the most popular MCMC technique which involves selecting a candidate point from a multidimensional proposal distribution representing the possible parameter values, and then comparing the likelihood of this point to that of the previously selected point. If the likelihood is higher then there is a higher chance of it being accepted and included on the posterior distribution. For SMC, importance sampling is popular, which instead uses weighted samples from the current source parameter estimate. These methods have been covered many times in literature, and so the reader is again referred back to Hutchinson et al. (2017) for a more detailed explanation of each method. The overall schematic for STE can been seen in Figure 6.

Within the realm of mobile robot STE, the primary differences between the proposed methods are the ATD models used, likelihood expressions, sampling strategies, and navigation strategies. Generally, any form of ATD model can be used within STE, however, some may be suited to certain environments better than others. As in most cases the algorithm is run on-board the mobile robot, the complexity and run time of the algorithm must be considered as a trade-off. The most commonly used ATD models for mobile robot STE are Gaussian plume (GP) models (Bourne et al., 2019; Magalhães et al., 2020; Rahbar & Martinoli, 2020; Rahbar et al., 2019a, 2019b) and IP models (Hutchinson et al., 2018, 2019; Ristic et al., 2017), both of which are

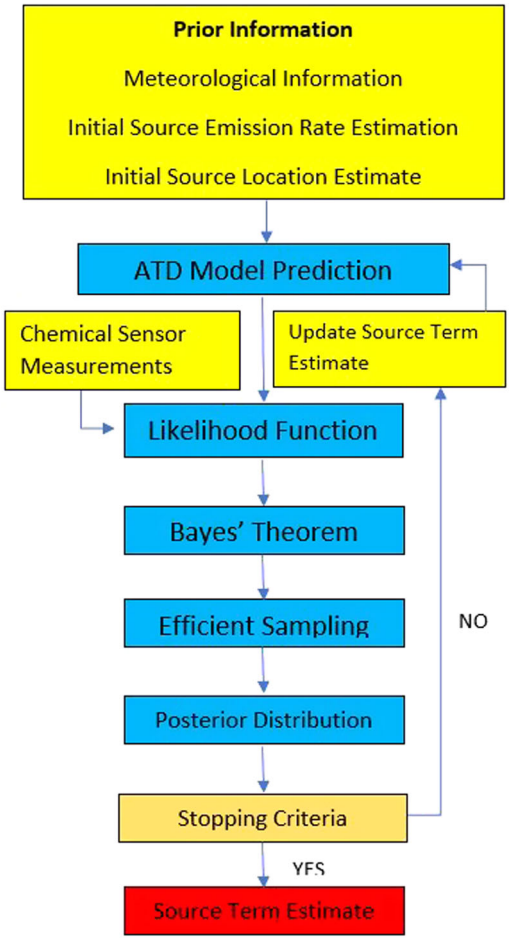

FIGURE 6 Source term estimation schematic [Color figure can be viewed at wileyonlinelibrary.com]

fairly simple and fast to compute. The performance of both models has been evaluated in open outdoor experiments using a UAV (Hutchinson et al., 2019). The results found that the IP model outperformed the GP model in small-scale experiments, suggesting that the IP model is more suitable for STE when the source location is not very far.

Likelihood functions

The role of the likelihood function is to give the probability of obtaining some concentration data D given a set of the ATD model parameters $\boldsymbol{m}$. This requires a method of linking the chemical sensor measurements with the expected concentration measurements. A likelihood function based on the work of Keats et al. (2007) assumes that discrepancies between measured and modeled concentrations are due to model and measurement error (Hutchinson et al., 2018, 2017; Rahbar et al., 2019a, 2019b). To encapsulate this error, a Gaussian distribution is used, as the principle of maximum entropy has shown it to be the most conservative (Jaynes, 2003). Whilst taking concentration measurements there is also the possibility of having a detection event (where gas is detected) and a nondetection event, where a nondetection event could be caused by various forms of error. A likelihood function for both possibilities can be defined, where a measurement is considered a nondetection event if the concentration does not surpass a threshold (Hutchinson et al., 2019). Errors considered for nondetection events include background and instrument noise, turbulence, and missed detections, or concentrations that include background and source contributions but do not surpass a threshold.

4.2.3 | Informative navigation strategies

To provide the inference phase with the most informative information, a navigation strategy can be implemented which compares the potential information gain from multiple possible measurement locations and selects the best estimated candidate. Considered as a partially observable markov decision process (POMDP) (Kaelbling et al., 1998), three components are required for the predictive navigation: a posterior distribution for the source parameters, a set of navigation actions, and a reward function. It should be noted that STE does not rely on an informative navigation strategy, as measurements taken from predefined sweeping trajectories have also given good results (Hutchinson et al., 2019). However, such an approach would require many concentration samples to be taken in large scale environments. Especially considering that ATD models often require time-averaged readings, the overall search time would be very long and might not be feasible for UAV platforms which have a limited flight time.

In Hutchinson et al. (2017), the principle of maximum entropy sampling (Sebastiani & Wynn, 2000) was used to choose the move that would give the most information. This was done through maximizing a PDF which considered the information gained about the posterior PDF given the new data, and the probability of the new data. Quantifying the measure of information was done by using negative Shannon's entropy which gave the uncertainty in the predictive distribution. The PDF was then approximated using a set of N samples for each possible movement, where the average information from the set of samples was used as the measure of the expected information. Simulations showed the algorithm to be able to be capable of finding the source location under high amounts of noise and under difficult starting locations, such as those located outside of the plume.

For a ground-based robot or UAV operating in 2D, a simple set of 4 navigation actions $\{\leftarrow,\rightarrow,\uparrow,\downarrow\}$ can be defined, where the information gain from taking a step in each direction is calculated by the relative entropy or Kullback–Leibler (KL) divergence between the current estimated PDF and the predicted PDFs. This approach was used directly by Rahbar et al. (2019a), however as it is purely exploitative, periods of no sensed chemical concentration (i.e., at the start of the search) would cause the robot stay in the same area for a long time. A new 2D movement vector was defined which weighted the sum of the exploitation vector with an exploration vector given by the maximum a posteriori value of the source position. The algorithm was found to work successfully when used on a UGV in

wind tunnel experiments, although increasing error was seen in lower wind speed conditions.

Inspired by the literature on optimal experiment design (Lindley, 1956), an approach by Hutchinson et al. (2018) used the probability of a future measurement with the KL divergence between the estimated and predicted PDF to define an integral reward function, representing the information gain from a potential next move. This required a set of possible future measurements to integrate over, which was computed using a Monte Carlo method utilizing the current parameter sample set. The strategy enabled a balanced exploration and exploitation search as it adapted with the PDF of the source parameters (more exploration at low uncertainties). When tested on a UGV in indoor experiments with a generated airflow, it was seen that the robot would perform crosswind casting in the presence of low information. Once uncertainty had reduced, it would travel more directly to the source in a similar fashion to biologically inspired anemotaxis. This suggests that STE may encapsulate the source searching strategies of nature whilst mitigating the limitations that arise from the use of an artificial sensor. In all trials, the source location estimate was typically within 10 cm of the true position.

To better balance exploration and exploitation, Chen et al. (2021) redefined the 2D STE navigation strategy from a control theoretic perspective. More specifically, the problem was formulated as a dual control problem, where the navigation aims at driving the robot to the target position (the source) while reducing the uncertainty associated with its belief. Named dual control for exploitation and exploration (DCEE), the algorithm aims to minimize a cost function that gives the expected error between the robot's future position from making a move, and the predicted estimation of the target position. The cost function consists of two parts: a part that drives the robot towards the target, and a part which quantifies the uncertainty of this predicted source location, therefore balancing exploitation with exploration. Both simulations and real experiments in an indoor environment with an UGV found that the DCEE was able to converge to the source location faster than two other methods: a purely exploitative classical MPC, and the explorative entrotaxis strategy.

4.3 | 3D algorithms for UAVs

GSL algorithms which localize a source within a 2D area are suitable for UGVs as they only operate on a single plane, however, UAVs offer the ability to operate in 3D, allowing them to exploit the whole plume phenomenon. Although 2D algorithms have been successfully implemented on UAVs in realistic outdoor experiments (Hutchinson et al., 2019; Neumann, 2013), a minimum navigation altitude must be set, which might not necessarily be the optimum value depending on the chemical source height and gas density. For a buoyant gas, an incorrect minimum altitude may cause the UAV to enter and leave the plume and incorrectly declare the source location.

Both bio-inspired and probabilistic single robot 3D algorithms have been proposed for use with UAVs. Although it is known that some biologically inspired algorithms are over reliant on a consistent chemical gradient, they are less computationally expensive than their probabilistic counterparts, are very reactive to changes in the plume, and do not require accurate localization. For these reasons, bio-inspired algorithms are still very much actively researched for use with UAVs (Ercolani & Martinoli, 2020; Eu & Yap, 2018; Shigaki et al., 2018; Terutsuki et al., 2021). They do however require a means of declaring once the source has been reached, which is a challenging problem in its own right. On the other hand, probabilistic algorithms such as STE encapsulate source location within the source term, and estimate other important source parameters simultaneously, providing benefits beyond source localization. They are however too computationally expensive to be used online with nano drones, require accurate localization, do not perform very well in low wind speed conditions, and require time-averaged gas concentration readings.

4.3.1 | Bioinspired 3D algorithms

The majority of early work on 3D GSL algorithms proposed extensions to 2D month-inspired algorithms, however, were only tested in simulation, or by using gantry-mounted robots. Edwards et al. (2005) proposed a 3D moth-inspired algorithm which used an internal timer to determine when the crosswind casting should occur. Two variations of the algorithm were proposed: a counter turner which reset the timer once the plume edge was found, and a modified counter turner which reset the timer upon detecting maximum concentration. The counter turner was found to perform the most successfully in small-scale experiments using a gantry-mounted robot and ion plume. More recently, Gao et al. (2016) proposed a 3D moth-inspired algorithm that makes use of a mobile robot equipped chemical sensors on the top, bottom, and on both sides of the robot. The pitch and heading of the robot is influenced by the local concentration gradient, however, this only applies during the upwind surge phase. Since the algorithm was only tested in simple simulations, it is not clear if the algorithm would work successfully in practical experiments due to the realistic limitations of chemical sensors. Use on a UAV platform would likely not be possible due to the difference in turbulence that would be experienced by the top and bottom-mounted sensors, greatly affecting their independent concentration readings.

The first evaluation of a 3D bioinspired algorithm in larger practical experiments was undertaken by Rahbar et al. (2017). Based on the 2D spiral-surge algorithm (Ferri et al., 2009), which performs straight line surges in the presence of the plume, and spiral casting once contact with the plume is lost, the 3D adaptation instead performs spiral casting on the Y–Z plane. In order for the algorithm to work successfully, a suitable gas concentration threshold was determined through using an approach based on advection-diffusion equations (Emery et al., 2017). This ensured that an

optimum value was chosen based on environmental conditions. Wind tunnel experiments with a gantry-mounted robot found the algorithm successfully locate an acetone gas source in all but very low wind speeds, giving an overall success rate of 70%. Again, since a UAV was not used as a robot platform, it is not clear if a gas concentration threshold value would be a suitable way of determining if the robot is in contact with the plume, as wake is likely to further dilute the detected concentration.

To evaluate the effectiveness of the 3D spiral-surge algorithm when using a UAV platform, Ercolani and Martinoli (2020) used an alternative sensing strategy based on sensing in motion. Such an approach reduces the effect of wake on the gas plume, as hovering to take time-averaged readings is not required. Due to the lower quality of the gas concentration measurements, the maximum concentration value within a sliding window was used to decide the next step. This limits the chance of missing a cue about plume's presence, which would likely happen if averaging was used. In addition, a smaller spiral drift constant was set to reduce the size of the spiral casts, as larger spirals would cause the drone to stay in the same area for longer, increasing the likelihood of losing the plume due to the drone's disturbance. In wind tunnel experiments using a nano drone, the source was located in all trials, however slower wind speeds and lower source emission rates negatively affected performance by slowing down the search and increasing distance overhead.

Although the spiral-surge algorithms discussed above allow for a 3D search, the spiral casting only occurs on the *Y*–*Z* plane. This method does not allow for a UAV located upwind from the chemical source to come in contact with the plume whilst casting. To overcome this, Eu and Yap (2018) proposed a moth-inspired algorithm with a spiral cast that varied on both the *X*–*Y* and *Y*–*Z* plane. In addition, a 3D zigzag cast was proposed and combined with the 3D spiral cast into one GSL algorithm. A combined strategy was chosen as the 3D zigzag cast was found to be more efficient at re-encountering the plume in the short time after contact with the plume has been lost, whereas the 3D spiral cast was faster at initially finding the plume, and at re-encountering the plume after a longer time. Although the algorithm follows the usual surge-cast style, stereo sensing was used to track the plume during the surge phase by using four MOX sensors located under each propeller. By angling the UAV towards the direction of highest concentration, the direction of the plume could be determined without using a dedicated wind sensor. Indoor experiments found that the 3D zigzag-spiral algorithm outperformed a 3D zigzag, and 3D spiral only casting algorithm. The results suggest that a combination of casting methods may provide a more robust GSL searching strategy.

4.3.2 | Probabalistic 3D algorithms

One of the first 3D probabilistic algorithms evaluated in both simulations and practical experiments was given in Ruddick et al. (2018). Based on the Infotaxis algorithm, the 2D plume model was replaced with a 3D GP model, allowing for the gas concentration to be estimated in 3D space. Two navigation strategies were compared: cross strategy, where the robot can move to an adjacent cell in any *XYZ* direction but in only one direction at a time (six possible targets), and Cube strategy, where the robot can move in any *XYZ* direction and also a combination of the three (26 possible targets). To decrease navigation time during straight line runs, an adaptive step length was applied when entropy was lower than a threshold. Although the Cube navigation strategy was more computationally expensive, simulations found it to be slightly faster at finding the source. Wind tunnel experiments found the algorithm to perform with a success rate of 100%, outperforming their previously tested moth-inspired algorithm (Rahbar et al., 2017). However, as the robot used in the experiments was again a gantry-mounted robot, further adaptations would likely be needed to achieve successful results when using the algorithm with a UAV.

In the 3D Infotaxis-based algorithm proposed by Ruddick et al. (2018), model parameters were assumed to be known before the experiments, which would not be true in real environments. To improve on this, they later estimated the model parameters through implementing an STE approach (Rahbar et al., 2019b). In a similar approach to their 2D STE method (Rahbar et al., 2019a), the navigation strategy was based on estimating the concentration in each of the possible target points, and then calculating the potential gain of information through using KL divergence. To allow for 3D navigation, six potential target points were again considered. Simulations of the algorithm found it to be robust to changing environmental conditions, however, they did not consider the effect of UAV wake on the algorithm's performance, as only a ground-based robot was simulated in a zero gravity environment. Furthermore, only a 2D version of the algorithm was tested in wind tunnel experiments.

To the authors' knowledge, the first example of a 3D probabilistic GSL algorithm tested using a UAV platform in outdoor experiments was undertaken by Hutchinson et al. (2019). Building on their STE method proposed in Hutchinson et al. (2019), an information-driven search strategy was used, instead of following a predefined sweeping trajectory to collect measurements. The search strategy relied on maximizing a utility function, based on their previous method proposed in Hutchinson et al. (2018). In a similar fashion to the above-discussed probabilistic algorithms, the utility function was evaluated for six potential target points, allowing for 3D navigation to be achieved. Outdoor experiments with a mini drone found the information-driven approach to locate a gas source in significantly less time and with more accuracy when compared to using a predefined trajectory. It was noted that variations in wind velocity did have an adverse effect on the performance of the algorithm, and longer sampling times would be required for more accurate estimations of source emission rates.

4.4 | Searching in structured environments

Much of the literature on mobile robot GSL focuses on source localization in open environments. In uncontrolled environments with

obstacles, it may be possible for Infotaxis and STE algorithms to ignore locations that contain obstacles by setting the measurements in those locations to 0, and then continuing to the next determined best sample location. This however leads to wasted navigation efforts, decreasing the search efficiency, and increasing the time needed to locate the source. In Ristic et al. (2014), an STE approach for GSL in unknown structured environments for robots equipped with SLAM was proposed. The search domain was modeled by a 2D lattice where the bonds/edges of the lattice represented traversable paths and breaks in the lattice represented obstacles. A Rao-Blackwellised particle filter was used to estimate the source parameters along with the search domain and location of the searching agent. The informative navigation strategy was based on calculating the information gain between the predicted PDF and the updated PDF over the state subspace using Bhattacharyya distance (Kailath, 1967). The algorithm was only simulated in simplified environments using a purely diffusive model, and so its performance in real scenarios remains unknown, however the numerical results indicated high success rates for the situations simulated.

More recently, Rhodes et al. (2021) proposed a 2D STE search strategy using Informed Tree Planning (ITP) to generate obstacle free trajectories between the robot and source location using a known map of the search space. Considering how obstacles affect the distribution of the plume, Dijkstra's search was used to produce a sample distribution where regions behind obstacles are less likely to contain chemical information due to the blocking effect on the particle's flow within the wind direction (Bellingham et al., 2002). The Entrotaxis reward function was used to determine which ITP trajectory would provide the most information gain, based on the possible future measurements. Having executed the chosen trajectory to record samples, the process repeats until the robot converges on the actual source location. Simulations comparing the performance of the standard Entrotaxis algorithm to the ITP algorithm within a CFD simulation of a source release found the ITP algorithm to far outperform the Entrotaxis algorithm. It could be seen that the Entrotaxis algorithm failed to locate the source within the simulation time frame, outlining the possible benefits of combining trajectory planning with GSL algorithms for use in feature rich environments.

Although the use of a known map of the environment allows for long term trajectories to be planned between the robot and estimated source location, often a map of the environment is not known until the robot has navigated the majority of the search space. To overcome this shortfall, Rhodes et al. (2022) proposed a 3D STE search strategy which combines DCEE with Rapidly Exploring Random Tree (RRT*) path planning to construct informative obstacle free trajectories. Localization was achieved using a stereo-inertial camera and the open-source ORB-SLAM3 SLAM method (Campos et al., 2021). A 3D voxel grid map representation was built using Octomap (Hornung et al., 2013), providing the robot pose and environmental map to the path generation process. Path generation begins with the generation of candidate trajectories using RRT*, where the maximum search distance is set to a sphere of radius equal to the maximum range of the camera. Following candidate resampling to reduce the number of possible trajectories, DCEE is applied to determine the most informative trajectory. Practical experiments were conducted using a mini drone in a 180 m^2 warehouse scenario containing obstacles and an acetone source. The gas source was successfully located in a time frame well within the flight budget of the UAV. As the underlying STE algorithm estimates the parameters of a time-averaged ATD model, it is not clear if the presence of obstacles had a negative effect on search performance, however the work is the first practical evaluation of an STE algorithm capable of GSL in cluttered environments, and a promising direction for the field.

4.5 | Gas source localization using estimated plume trajectory

Although Infotaxis and STE algorithms have proven to be successful in localizing chemical sources in turbulent environments, wind velocity is often assumed to be constant, or to not vary too far from its estimated value. Large changes in wind speed and direction are likely to cause rapid degradation in performance and increased uncertainty (Rodríguez et al., 2014). Recently, approaches to GSL have been proposed which instead estimate the probability that the plume has traversed through a certain area and use this to guide their navigation strategy towards the source.

A 2D approach was proposed by Li et al. (2019) which used the mean airflow velocity over a short-time scale to plan a navigation strategy by estimating the path of the plume, referred to in their work as the chemical-patch path (C-PP). Assuming homogeneous airflow, the probability that a detected chemical patch came from a location is represented by a PDF, where the movement of the plume is modeled as a random walk superimposed on the mean wind velocity measured over a short period. Locations of probability above a threshold are used to estimate the possible area that the C-PP traveled through (Li et al., 2011). This area allows the navigation strategy to plan two sub-routes within the C-PP: an upwind route and a downwind route. The upwind route is prioritized, however if no more chemical detections are made whilst exploring this route, the robot turns back to follow the downwind route to check remaining C-PP areas. If a detection is made, a new C-PP is estimated and therefore two new sub-routes. This iterative search allows the robot to eventually converge on the source location whilst considering new wind information with each iteration. Outdoor experiments conducted in a large open area showed consistent success, even though wind direction during the experiment varied between 107° and 260°.

The assumption of a homogeneous airflow may not hold in environments with obstacles, therefore Ojeda et al. (2021) instead estimated the probability that the plume had traversed through an area in close proximity to the robot using local wind and chemical measurements, and then propagated those measurements through the 2D search space. By breaking the search space into cells, a wrapped normal distribution was used to model the probability in adjacent cells, which was maximum for the cell directly upwind and symmetrically less for cells further away. If no chemical is detected,

an assumption is made that the robot has moved in the wrong direction, so the wrapped normal distribution is instead centered at the direction of the last hit, rather than using the wind direction. By using an 8 neighbor propagation algorithm, the probability of the source being in the rest of the cells is modeled based on the shortest free path, therefore conforming to the geometry of the environment and recursively updated using Bayes theorem. Simulations and real-world experiments of two navigation strategies using the estimation algorithm showed better success rates than a reactive Surge Cast algorithm, mainly due to single missed detections causing less of an effect on the exploration. However, it was noted that this causes the robot to take longer to react to changes in plume direction, as multiple cells would need to be searched before making a turn.

5 | GAS SOURCE LOCALIZATION WITH MULTIPLE ROBOTS

Mobile robots offer a flexible solution to localizing chemical sources as only a single sensing node is required. However, much research has been put into developing algorithms where multiple robots can be used to localize chemical sources through cooperative searching. The use of multiple robots allows for a greater area to be searched more quickly and can improve the overall searching efficiency. Such approaches are beneficial for UAVs, which can only collect a limited number of samples due to the additional energy used from hovering to take measurements. Through distributing the sampling task across the robot team, greater areas can be searched before their battery is depleted.

When considering a cooperative multirobot algorithm, considerations need to be made on how to fuse the sensor information gathered from each individual agent to guide the navigation strategy of the robots. One method is to have a centralized approach, where each robot can share its coordinates of plume encounters and readings with the other agents to inform their decision making. For STE, this would cause each likelihood function in the robot team to be updated with the new information. Although each robot calculates the PDF independently, all the available information is the same for every robot and so the centralized fusion is replicated. This would effectively increase the detection rate of the team, decreasing the time needed to estimate the source location. In decentralized approaches, estimation, motion planning and control are performed by each individual robot (Durrant-Whyte, 2000). Robots are still influenced by the observations of other robots, however continuous communication between robots is not as necessary.

5.1 | Formation-based approaches

In formation based searching, the team of robots remain in a set formation throughout the search. As robots remain at a set or minimum distance from other robots in the team, collision concerns between robots are mitigated. Remaining in a formation can also allow plume tracking to be accomplished more easily, as the robot formation can be centered on the plume gradient.

Lochmatter et al. (2013) proposed a "crosswind formation algorithm," which focused on keeping robots on the left and right side of the odor plume by ensuring the average chemical concentration was the same on both sides. Each robot used within the formation could detect and measure the chemical concentration along with the wind direction relative to their pose. The robots share this information with all robots within the formation. Each of the robots' wheel velocities were determined by calculating a virtual crosswind and upwind force, denoted as f_c and f_u, respectively. The forces ensure that the robots stay aligned with a downwind distance from the source, and keep the robots centered on the plume with a certain distance from each other. In experiments conducted in a 16x4m wind tunnel, robots were able to locate a chemical source 100% of the time, even when the initial starting position of the robots was moved between 3 different sides of the wind tunnel. In realistic scenarios without a strong continuous airflow, it is unlikely that such an approach would yield successful results, due to the realistic intermittency of the plume.

Li et al. (2014) proposed a control-based cooperative gradient climbing algorithm, where the gradient was estimated analytically using a least square estimator. The underlying control law aims drive the robot towards the source with a gradient climbing behavior, whilst simultaneously keeping the robot team in a desired formation on a 2D plane. Two communication strategies were compared: an all-to-all communication strategy where robots share their observations with all other robots, and a scalable limited communication strategy where robots only communicate to their neighboring robots. The underlying control laws of both strategies were similar, however the limited communication strategy relies on distributed consensus filters to estimate the centralized quantity in the control law. Practical experiments using a team of three UGVs found that the all-to-all strategy was faster at converging to the source location and took a more direct route, however both algorithms were able to locate the source successfully. It should be noted that a light source was used in the experiments rather than a chemical source, meaning that a continuous gradient would be measured. Further modifications would be needed to allow for a chemical source to be located, due to the differences in sensor response and gradient consistency.

A 2D formation-based algorithm was proposed by Ristic et al. (2017), where a vector of each robot's sensor measurements and positions was used to estimate the source parameters through STE. Searching was conducted in a circular formation, where robots use the source location PDF to guide an information-driven search. A robot movement model ensures that the robots to stay in formation. The movement model relies on a vector of 4 parameters: linear velocity, angular velocity, formation scale, and travel time. The parameter vector is chosen from maximizing a reward function that considers the expected reduction of entropy from a movement and the cost incurred due to the distance traveled. The scale parameter allows the formation to expand or shrink, however there are maximum and minimum limits imposed to ensure that the robots

do not break communication or collide. Simulations of the algorithm found the source finding success rate to be 100%, and that increasing the number of robots gave diminishing performance gains.

Building on the formation algorithm in Ristic et al. (2017), a decentralized version was proposed in which each robot within the formation computes the source estimation and motion control independently from other platforms (Ristic et al., 2020). Although in this case, the robots within the formation share their measurements and positions with neighboring robots to construct their source parameter PDF. This makes the approach scalable as complexities in communication and computing are independent of the robot formation size. As a particle filter was used to compute the posterior, the independent PDFs might not necessarily be the same, making the approach decentralized. Therefore, the robots may not agree on the most infotactic formation movement. To avoid formation break-up, a decentralized cooperative control based on average consensus was applied (Ren et al., 2007), allowing for an agreed motion to be decided. Simulations found that increasing the number of platforms decreased the search time dramatically, however the decrease in source localization accuracy did not fall quite so substantially.

5.2 | Centralized approaches

A centralized 2D multirobot Entrotaxis algorithm was proposed by Ji et al. (2021), which aimed to achieve CSL in large-scale chemical clusters. Adaptations to the Entrotaxis algorithm were made to limit robot navigation to existing roads to avoid industrial obstacles. As the robots are constrained to roads, if the robot cannot move in its desired direction to reach a planned sample location after m steps, the robot performs a long-distance turning movement whilst not taking new sensor measurements. If the robot reaches an intersection, it can then turn to its original desired direction and continue taking measurements. Simulations using a CFD model of a source release on a chemical cluster scene showed that even though plume distribution varied across the site due to interactions with obstacles, robots were able to locate the source with high accuracy. The use of multiple robots improved localization accuracy and decreased the required navigation steps when compared to the results from a single robot.

Bourne et al. (2019) proposed a centralized 2D STE approach where sensory information is shared with the whole robot team, however robots are assigned separate headings/goals to encourage exploration. A bio-inspired motion planner was proposed which used the analytical gradient computed from the Gaussian plume model of the STE algorithm. Coordination between robots was achieved by instructing each robot to investigate a different mode/hypothesis from the multimodal posterior. Different modes are likely to express different wind and analytical gradient estimates, therefore robots work together to find the correct source term over time. Indoor experiments were conducted to test the distributed algorithm, where a humid air plume was used to represent a gas source. It was found that the coordinated approach was roughly twice as fast as an uncoordinated approach, robust to changes in the plume, and to variations in initial positions.

To further verify the advantages and constraints of a coordinated STE approach, Rahbar and Martinoli (2020) compared three coordinated strategies with varying levels of collaboration. The first strategy consisted of the most basic level of coordination, where robots search independently to each other. If one robot declares it has found the source, then all robots stop. The second strategy followed a standard centralized approach, where sensory information is shared between the robot team. MCMC sampling is used in the STE by each independent robot, meaning a slightly different PDF can be held by each robot, and therefore different opinions on the next best move. In the third approach, sensory information is shared between robots and movements are coordinated between the team. If a robot's opinion on the next goal position is closer to another robot, then the robots swap goals to reduce the overall distance traveled by the team. Wind tunnel experiments using a team of UGVs and an ethanol source found that with increasing levels of cooperation and number of robots the trial duration would decrease. Robots would also begin to take smoother trajectories towards the gas source. As the algorithm was only tested in wind tunnel experiments with a single wind profile, it is not clear if as much success would be achieved at lower or more unstable wind speeds. However, the results suggest that cooperation between robots improves overall performance when compared to uncoordinated or single robot search strategies.

5.3 | Decentralized approaches

Although a centralized STE communication strategy does allow for a faster reduction in source location uncertainty, simulations by Hajieghrary et al. (2016) found that this would come with the downside of false positives from incorrectly estimating the source location when variance in the source position estimate dropped below a threshold. This would cause robots to converge onto a wrong location and move only when limited chemical encounters were detected, delaying the search, or incorrectly declaring the source. They instead proposed a decentralized strategy where each robot maintains its own source PDF estimate, updated only with its own information. Each robot chooses its next sample position based on the reduction of relative entropy between its own PDF and that of other agents using KL divergence. Simulations for the proposed strategy found that although inefficiencies may come from robots visiting the same positions twice, a more successful search was conducted which did not sacrifice estimation quality. Basic simulations by Karpas et al. (2017) also found the strategy to result in an efficient source localization search, outperforming the performance of non-cooperating agents.

Many of the discussed multirobot STE algorithms have only tested in simulation or in smaller indoor environments where lapses in communication between robots are less likely. In larger outdoor environments, lapses in communication are a common occurrence, meaning that coordination between robots should be achievable with as limited communication as possible. Such an approach was taken in Bourne et al. (2020), where coordination between robots was

achieved with belief sharing. This way, robots within the team maintain their own beliefs on the source term and choose their own informative waypoints, but share their beliefs with the rest of the team on occasion. This has the benefit of correcting drastically different beliefs across the robot team, or for when prior distributions vary. In outdoor experiments over a 50 × 50 m area, a team of five mini drones were able to successfully locate a propane source within 5 m of the true location. The results demonstrate that cooperative searching can aid in GSL over large areas for UAVs with limited flight time.

5.3.1 | Particle swarm optimization (PSO)

One of the most commonly investigated multirobot techniques is PSO. PSO is an optimization technique which finds a candidate solution and improves it over time by iteratively updating it, eventually converging to an optimum (Eberhart & Kennedy, 1995; Kennedy & Eberhart, 1995). In the typical PSO algorithm, each robot is considered as a particle, where its velocity at a given time is determined by its own observations and the observations of other robots. Once a robot has found a location where the pattern is better than any previously found, it stores it in a local best position variable. The difference between the local best position and the robot's current position is stochastically appended to the robot's current velocity, which causes a change in the robot's trajectory. The difference between the global best position and the robot's current position is also weighted and added the robot's velocity. This adjusts for the next iteration, which causes the robots search behavior to tend around the two best positions. The adjustments to the algorithm cause a flocking behavior at the most likely locations, similar to the behavior of birds when food has been discovered. PSO is applicable to both 2D and 3D searching (Lee et al., 2018), making it suitable for use with UAVs.

For use in gas source localization applications, other considerations must be made for PSO to work successfully. Particles (the robots) can become trapped at the local optimum, therefore Jatmiko et al. (2007) proposed a charged PSO (CPSO). In CPSO, some robots are given a charge, while others are considered as neutral. Charged robots would have a mutual repulsive force between them, preventing them from becoming trapped in a local maximum location, whilst neutral robots would act in the normal way. Later, adaptations were made to fuse local wind information with the robot velocity, allowing the robots to follow the gas plume gradient upwind (Jatmiko et al., 2009). Other attempts to prevent trapping at local maximums have included randomizing the constriction factor used in the exploration term of the velocity command (Eberhart & Shi, 2001), or by linearly decreasing it (Eberhart & Shi, 2000). As local maximum areas of chemical concentration can be located at positions away from the source, a probability-based PSO algorithm (P-PSO) was proposed and simulated in Li et al. (2008), which instead expressed the fitness function as probability using Bayesian and variable-universe fuzzy inferences. P-PSO was later evaluated in indoor experiments using a team of UGVs (Meng et al., 2011), which found that the algorithm worked reliably in time-variant airflow environments, except when airflow was extremely dynamic.

One of the first examples of PSO in large outdoor experiments was given in Steiner et al. (2019). An alternative PSO strategy was proposed where waypoints are set for the robot to navigate towards, in comparison to using the velocity command. This has the benefit of allowing for a lower frequency of communication between robots, and makes obstacle avoidance using LiDAR more feasible, as robots were found to struggle avoiding obstacles when the velocity command continuously changed. Simulations found the waypoint-PSO strategy to outperform the standard implementation, due to only a small proportion of the search space containing chemical concentration. Robots using the velocity-PSO implementation would get stuck swarming in the center of the search space due to no agents detecting an initial concentration. Following the simulations, the waypoint-PSO strategy was tested in practical outdoor experiments using a team of three mini drones. When localizing a propane source, the greatest level of chemical concentration was detected 19 m away from the source. UAVs flew close to the source on occasion, however, did not detect any concentration. This could be caused by the limitations of the chemical sensor, which was implemented in a passive approach on top of the UAV, and from the effect of wake on the sensor response.

A similar waypoint-style PSO algorithm has also been implemented on nano drones to locate a chemical source in indoor experiments (Duisterhof et al., 2021). Nano drones may cause less of a disturbance to gas plumes in comparison to microdrones, but they require smaller and simpler obstacle avoidance sensors to allow for navigation in cluttered environments. For this, laser range finders were used to allow for a simple bug algorithm to be used for local obstacle avoidance. Waypoints were generated using the sum of the robot's velocity vector (calculated with PSO) and its current position. The navigation strategy consisted of three phases: line following, wall following, and attraction–repulsion swarming. Line following occurs when no obstacles are detected, the agent then follows a direct line towards the goal waypoint. Wall following occurs when an obstacle is detected, initiating the bug algorithm. Attraction–repulsion swarming occurs when another robot comes within a minimum distance of the robot's position, which causes a new velocity command to be generated. In practical experiments using a team of three nano drones, an alcohol source was located in 11 out of 12 runs. The failure was due to the drones converging on a local optimum. For future 3D extensions, alternative obstacle avoidance strategies would be required to allow for variation in altitude.

5.4 | Localizing multiple sources

Rather than assuming the number of sources before the search, a multirobot infotacic algorithm was proposed by Wiedemann et al. (2017), which used sparse Bayesian learning (SBL) to incorporate the uncertainty on the number of chemical sources. Finite difference

method was used to transform a partial differential equation 2D diffusion model into a finite number of grid cells, along with aggregating the source strength for each. By exploiting the assumption that the chemical sources were few and sparsely located in the search space, SBL was incorporated which uses a parametric before determine if an element of source locations contain a source or not. The exploration strategy considered cells that had high variance for the estimated source marginal PDFs to be of high uncertainty, and so each robot selects a cell to sample next based on the uncertainty weighted with the distance between the cell and its current position.

The algorithm was improved further to use a distributed implementation, where a factor graph (FG) was used to model the relationship between the random variables (Wiedemann et al., 2017). The FG provides a foundation for message passing algorithms, where messages are sent along the edge of the graph between factor nodes and variable nodes. The outgoing variable node messages eventually converge to the corresponding parameter or variable's marginal distribution through the iterative exchange of messages (Wiedemann et al., 2018). By dividing the overall FG into different parts, robots can be assigned to different regions to calculate messages of their own part and exchange messages along the border with neighboring agents. Robots are not limited to their own areas and can visit any cells that are deemed to be of low uncertainty, however, a penalty is applied for far away locations. Practical experiments using a simulated diffusive source showed that the algorithm was able to locate the source after 230 measurements, outperforming a meandering strategy which converged after 340 measurements.

To evaluate if the sparsity-inducing prior was beneficial, Wiedemann et al. (2019) simulated the algorithm's performance with and without the sparse prior. They also replaced the 2D diffusion model with a 2D diffusion-advection model, allowing for a wind before be used. The results showed that using the sparse prior led to lower error in less iterations. It was also found that an inaccurate wind prior did not cause too much degradation in performance, as long as the error in wind direction did not exceed 30°. This inspired further real experiments, where a team of UGVs successfully localized two ethanol sources in an indoor environment where an artificial airflow was present (Wiedemann et al., 2021).

6 | GAS DISTRIBUTION MAPPING (GDM) WITH MOBILE ROBOTS

GDM is a task of creating a map of the distribution of an airborne chemical over an area of interest through gathering spatially distributed chemical measurements. The mobile robot can only sample so many points within an acceptable time frame, and so the sparse measurements along with fluctuations in chemical concentration make this a difficult task (Rhodes et al., 2020). In comparison to chemical localization algorithms which attempt to navigate to the chemical source location, GDM algorithms often require the robot to follow a predetermined trajectory whilst periodically gathering concentration measurements. Some GDM algorithms use gas distribution models (Fukazawa & Ishida, 2009), such as those derived from turbulent diffusion theory (Ishida et al., 1998). However, such GDM algorithms can be overly simplistic and can cause gas distribution to be inaccurately modeled due to assumptions of steady and uniform airflow throughout the search space. Model-based approaches do however have benefits in open areas where their underlying assumptions hold, and therefore a recent example is discussed in the following section. Model-free approaches which do not make strong assumptions about the distribution of gas are a generally more robust choice for a variety of environments, and therefore will be the focus of this section. GDM algorithms can provide a richer understanding of the gas distribution over an area of interest, however, come with the downside of a longer search time, due to the number of samples needed to provide high-quality maps.

6.1 | Kernel distribution mapping (DM)

The Kernel DM algorithm presented by Lilienthal and Duckett (2004) is a model-free approach which uses a Gaussian weighting function to model the decreasing likelihood of a particular reading representing the true concentration with respect to distance from point of measurement. It is a 2D grid-based strategy, where a mobile robot generally performs a sweeping trajectory covering the majority of the area of interest. Periodically sampled measurements are corrected with baseline manipulation and normalized. For each cell within a cutoff radius R_{co}, a weight is assigned by using the displacement to the grid cell's center to solve the Gaussian weighting function. Finally, the value of a cell is set if the sum of the weighted readings divided by the sum of the weights exceeds a threshold. The total algorithm relies on three parameters: the cutoff radius R_{co}, the threshold value W_{min}, and the width of the Gaussian function. Choosing a suitable width is critical to ensure that the map preserves the fine details of the mapped structures but remains high enough to give sufficient extrapolation. The Kernel DM algorithm provides means to map the chemical concentration distribution but does not take into account fluctuations in detected chemical concentration which has suggested to be a reliable marker of source proximity (Fackrell & Robins, 1982; Justus et al., 2002; Mylne & Mason, 1991; Yee et al., 1994).

6.1.1 | Kernel DM+V

An important improvement to Kernel DM to account for variance was later proposed in Lilienthal et al. (2009). The algorithm requires three temporary grid maps: a map of integrated importance weights, integrated weighted readings, and integrated variance contributions. The final mean and variance maps are calculated using the weighted and confidence maps. The algorithm relies on three parameters: a kernel width parameter, a cell size parameter, and a scaling parameter for the confidence map. The cell size determines the resolution at which predictions can be made, and the scaling parameter defines a

threshold between values which are considered high or low. The kernel width determines how much extrapolation on individual readings is applied. The algorithm was validated in real experiments where a UGV was made to follow a sweeping trajectory around an outdoor area with a gas source located in the center. Chemical concentration measurements were taken at predefined grid points. The mean gas distribution map showed a region of high concentration in the top left quadrant of the search area, possibly caused by the wind direction during the experiment. The variance map showed a clear high region of variance at the center of the map where the chemical source was located. Although the variance map shows the location of the source more clearly, the distribution map is still useful in determining any regions of high chemical concentration which could be deemed as hazardous. This property was explored in Bennetts et al. (2016) by using a mobile robot and the Kernel DM+V algorithm to find regions of high pollution within a steel works foundry. The results of which showed regions within the foundry that were more prone to accumulating dust and pollution. It was concluded that the robot could help in determining the placement of static sensing nodes to allow for continuous monitoring of such areas.

6.1.2 | Kernel DM+V/W

An extension to the Kernel DM+V algorithm was proposed in Reggente and Lilienthal (2009) which used local wind measurements to more accurately model the chemical distribution. The modified algorithm, known as the Kernel DM+V/W replaces the univariate Gaussian kernel with an elliptic multivariate Gaussian kernel. The shape and orientation of the kernel is correlated to the local wind velocity, allowing for the information on where the chemical has come from and where it is likely to go to be incorporated into the algorithm. Outdoor experiments were conducted with a UGV equipped with an E-nose and an ultrasonic anemometer. The results showed a clear improvement in how the algorithm was able to estimate unseen measurements over Kernel DM+V when the wind was present. The algorithm has also been implemented successfully using measurements taken with a mini drone (Neumann, 2013). An extension to allow for 3D mapping has also been proposed through utilizing a 3D Gaussian kernel (Reggente & Lilienthal, 2010). Although a UGV was used to test the algorithm using an E-nose with sensors located at three different heights, the algorithm would also be applicable for use with UAVs, so long as considerations were made to reduce the additional sensor noise.

6.1.3 | Kernel DM+V for multiple different sources

To account for the possibility that many different types of gas sources may be present, a Multicompound Kernel DM+V algorithm (MC Kernel DM+V) was proposed in Bennetts et al. (2012), and later improved in Hernandez Bennetts et al. (2014). The algorithm uses a set of posterior probabilities given by a chemical discrimination classifier computed from measurements taken with an array of MOX sensors. For each chemical, three maps are sequentially produced: a classification map, mean concentration map, and predictive variance map. An example of the results produced by the MC Kernel DM+V algorithm can be seen in Figure 7, for a situation where two gas sources where present. The classification map shows a higher probability of detecting a specific compound in regions where the neighboring data points were classified with high confidence. The mean map shows regions where high chemical concentration is likely to be encountered due to the different gas sources. The variance map shows two clear high regions of variation at the locations of the sources which is as to be expected, allowing for the locations of the gas sources to be located easily. Although it is ideal to have the robot patrol and gather samples across the entire area of interest, the MC Kernel DM+V algorithm can estimate the gas distribution from multiple different sources even when using sparsely gathered samples, making it useful for time-sensitive emergency response scenarios (Fan et al., 2019).

6.1.4 | Plume model-based kernel mapping

The Kernel DM+V/W algorithm uses a bivariate normal distribution, where the shape that governs the amount of extrapolation is determined by the local wind velocity. This better accounts for the effect of wind on the gas distribution, however, the stretching parameter of the algorithm must be set manually or empirically. In recent work by He et al. (2019), the bivariate normal distribution was replaced with a GP plume model. The GP model provides concentration prediction further downwind, and with a physical explanation for its estimates. Furthermore, the diffusivity parameters of the model can be set based on the environmental conditions using Pascquill stability classes (Steinfeld, 1998). Simulations found the modified algorithm to map a series of simulated plumes with less error than both the Kernel DM+V and Kernel DM+V/W algorithms. Real-world tests were conducted in a salt flat environment using three mini drones. A propane source was used to produce a gas plume. To map the area more quickly, each mini drone simultaneously collected measurements in a lawnmower sweep over 1/3 of the test area. Due to the dilution of the chemical concentration caused by the mini drones' wake, and from the limitations of the chemical sensors themselves, only the mini drone nearest to the source was able to detect a chemical concentration. Regardless of this, the GP plume model was still able to provide information further downwind, even though no concentration was detected in that region. It should be noted that this environment perfectly suits the underlying assumptions of the GP model, however, in obstacle-rich environments the plume is likely to become distorted, leading to inaccurate modeling.

6.2 | Gaussian process regression

An alternative approach to gas distribution mapping is to use machine learning to find a model which best explains the observed

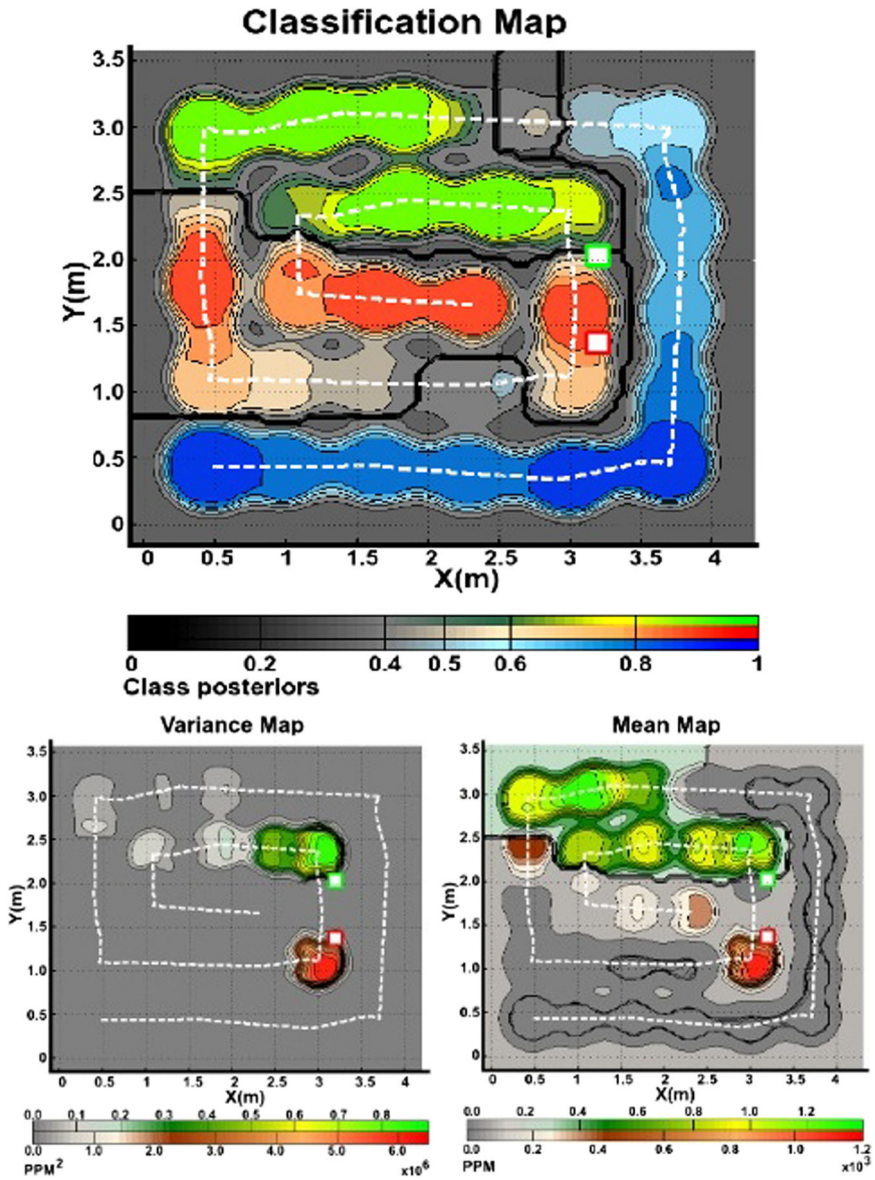

FIGURE 7 Classification, mean, and variance maps produced using the MC Kernel DM+V algorithm for an area which includes two chemical sources. Green represents ethanol, red represents propanol, and blue represents the likelihood of finding clean air. Adapted from Hernandez Bennetts et al. (2014). Licensed under CC BY 3.0 (https://creativecommons.org/licenses/by/3.0/). [Color figure can be viewed at wileyonlinelibrary.com]

measurements, and to accurately predict the concentration in unmeasured regions. GPR is one such method which has been actively used to produce GDM using mobile robots. A detailed introduction into GPR can be found in Rasmussen (2003), although a basic description of GPR is given in Section 2.5.5, within the discussion of the gas quantification algorithm proposed by Monroy et al. (2013). A drawback of GP regression is that it is computationally expensive when compared to the lightweight Kernel algorithm discussed above.

For mobile robot GPR GDM, stationary covariance functions are primarily used as nonstationary functions are difficult to apply, often requiring more prior knowledge than is available or can be assumed (Gosmann & Opper, 2013). The most common stationary covariance functions are the squared exponential covariance function with and without automatic relevance determination (Marchant & Ramos, 2012; Stachniss et al., 2008), and Matérn class covariance functions (Stachniss et al., 2009). Squared exponential covariance functions are better at modeling smooth functions, and therefore have a greater smoothening effect on the resulting chemical distribution maps. Matérn class covariance functions are less smooth, and so can provide rougher estimates. The performance of the two was investigated in Stachniss et al. (2009) which found the Matérn class covariance functions to perform slightly better than the squared exponential, as the lesser smoothness seemed to fit better with the nature of gas distribution.

6.2.1 | GP mixture models

An improvement to the standard GPR GDM algorithm was proposed by Stachniss et al. (2008) to account for the smooth background noise and areas of high concentration found in real environments by using a GP mixture model. In the standard GPR approach, each location is represented by a unimodal distribution, where background

noise is mixed with the real concentration. The GP mixture model is instead composed of the locally weighted sum of the multiple GPR models. To reduce computational complexity, a reduced set of the training data was used, in a similar method to that of Sparse GPs (Smola & Bartlett, 2001). The algorithm was tested by comparing its performance with the standard GPR approach by using data collected by an E-nose equipped UGV in indoor and outdoor environments where a chemical source was present. Better modeling of the predictive mean was seen near the source location, as the standard GPR was seen to apply too much smoothing. The predictive variance map showed regions of high variance near the source, improving over the standard GPR which showed no obvious regions of uncertainty due to the assumption of constant noise for all inputs.

6.2.2 | Effect of noisy training data on model prediction

Many experiments that evaluate GDM algorithms are conducted in uncontrolled outdoor environments, where airflow is likely to change over time causing the distribution to vary. The maps that are produced use sensor data for point measurements, which are collected over a large time frame and do not represent a snapshot of gas distribution. This makes it impossible to achieve repeatable results in such experiments to properly evaluate the algorithm's performance. This motivated Hutchinson et al. (2019) to create a ground truth data set by producing a consistent chemical distribution in an indoor controlled environment to benchmark the performance of GPR GDM. This was achieved by using fans at either side of the room to generate a constant wind field along with a source of acetone which was dispersed with a heat gun. A UGV equipped with a PID chemical sensor was then made to perform a sweeping trajectory along the test area to gather measurements. It was found that 30 s sampling time achieved repeatable results, and so the data set produced was used as a ground truth. Sampling times of 5 and 1 s where then compared to represent the typical noisy training data gathered in real experiments. It was found that 5 s produced results with much less error. When compared with two other regression methods (neural network, and piecewise linear interpolation), GPR was found to have better prediction quality at the expense of additional computational complexity. The GPR GDM algorithm was then used on a data set collected by a mini drone in uncontrolled outdoor experiments which featured an acetone source. It could be seen that the area of highest concentration was located slightly to the right of the actual source location, most likely due to effect of wind flow.

6.3 | Gaussian Markov random fields (GMRF)

The GDM methods mentioned thus far all assume that no obstacles are present in the area of interest. This is fine for open outdoor spaces, however for cluttered or indoor environments, gas distribution is strongly affected by obstacles. Another thing to consider is the age of the measurement samples. Due to the mechanisms of gas dispersion, odors should be considered as ephemeral (Shraiman & Siggia, 2000), meaning they weaken as time goes by. As the measurements sampled by the mobile robot are taken over a long time frame (dependant on area size, number of samples, and sample time), older measurements should not hold as much weight as newer ones (Asadi et al., 2011). A new algorithm proposed by Monroy et al. (2016) considers both these problems through spatially modeling the gas distribution on a 2D lattice using GMRF. GMRF is the most recent attempt at GDM which is novel in that it considers the age of samples and obstacles within the environment, therefore its methods and results will be described here in detail.

The goal of GMRF is to find the maximum a posteriori estimate for chemical concentration in each cell along with its uncertainty, given the sampled observations and some prior knowledge of how the gas spreads over the area, and how obstacles affect the gas propagation between close-by cells. A factor graph is used to model these dependencies, where nodes represent estimated chemical concentration at a cell, or the chemical observations. FG edges represent factors between nodes: observation factors (the relationship between observations and the true chemical concentration), and prior factors (the behavior of the spatial chemical distribution). The goal is to achieve a joint probability distribution for that cell using the two different sets of factors. Each observation is modeled as having an increase in uncertainty with a Gaussian error, based on the time the observation was made. If an obstacle is present, then it is assumed that there is no correlation between the cells (essentially removing the edge between nodes, see Figure 8). To estimate the MAP, the GMRF is entirely defined in a Jacobian matrix, allowing for the uncertainty to be recovered through performing the inverse of the Hessian.

The performance of GMRF was evaluated in simulation and compared to the Kernel DM+V approach in an environment with rooms. A chemical source was located in one of the rooms which was turned off partway during the simulation. Two key things were apparent, the GMRF was able to model the chemical distribution within the bounds of the room, whereas Kernel DM+V does not take this into consideration. Also, once the source has been switched off, the GMRF no longer modeled a chemical concentration in that room, whereas the Kernel DM+V did, however, the mean concentration was weakened (due to its averaging effect). This suggests that GMRF is able to react quickly to the changing environment by giving newer observations more weight. When the situation was recreated in practical experiments, similar outcomes were witnessed, however, once the source had been turned off GMRF did still show a mean distribution in the room, probably due to there being some residual gas concentration in the air. The algorithm is however far more computationally expensive, as execution time is dependent on map size, whereas Kernel DM+V is almost independent.

6.3.1 | Joint estimation of chemical and wind distribution

GMRF has shown to provide a means to map chemical concentration whilst considering the effect of obstacles and observation age,

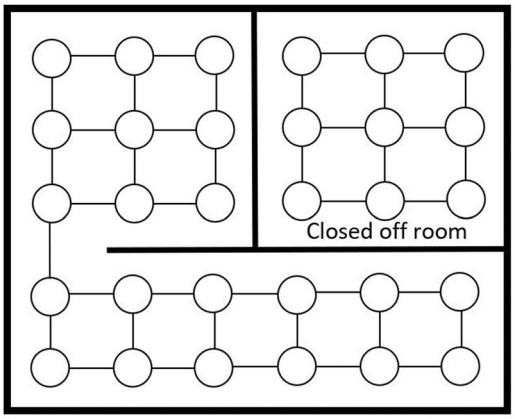

FIGURE 8 Example of a MRF in which nodes are the chemical concentration at cells, edges are the relationships between adjacent nodes. Observations and factors are not included for the sake of clarity.

however it does not consider the effect of wind on the chemical distribution. The Kernel DM+V/W on the other hand takes wind into consideration but uses local wind observations to model its effect. GMRF has previously been used to solve wind distribution maps (Monroy et al., 2017), therefore Gongora et al. (2020) proposed jointly estimating chemical and wind distribution maps to make reasonable assumptions about the chemical distribution in unexplored regions. This would allow for less measurements to be needed, speeding up the mapping process. Wind observations would be in the form of a 2D wind vector at a given cell, sampled with an anemometer. Observation and prior factors were modeled as energy functions and calculated separately for both wind and chemical maps following a similar strategy as the standard GMRF. The mutual influence of the two maps on the chemical distribution was solved by computing the joint probability distribution of the two maps. Practical experiments found the algorithm to work well, however, it was noted that it was considerably more computationally expensive when compared to standard GMRF or Kernel DM+V/W. In environments with little airflow, the algorithm's ability to extrapolate measurements is limited, which should be kept in mind when deciding on suitable applications.

6.4 | Adaptive path planning strategies

When collecting samples for GDM, nonadaptive path planning strategies are typically used, where the robot follows a preplanned trajectory and periodically takes measurements. The most commonly implemented strategy is to follow a sweeping "lawnmower" style trajectory, allowing for samples to be taken over the majority of the search space (Bing et al., 2015; Lilienthal et al., 2009; Neumann et al., 2012; Reggente & Lilienthal, 2009). This is a time-consuming process if an accurate distribution map is to be produced, as was noted by Neumann et al. (2012), who found that the limited flight time offered by the mini drone used in their experiments would greatly limit the area that could be mapped with a nonadaptive strategy. A recent direction for the field is to use adaptive path planning strategies that compute sampling locations online. Known as informative path planning (IPP), the problem is challenging due to the time-variant nature of gas dispersion, and due to the effect of the robot's trajectory on the gas distribution. Compared to UGVs, UAVs will introduce further disturbances due to the additional turbulence from their propellers.

One of the first attempts to combine IPP with GDM was given in Neumann et al. (2012), where the Kernel DM+V/W algorithm was used for GDM in combination with an artificial potential field (APF) IPP. As Kernel DM+V/W provides both a mean and variance map, regions of high mean and variance were given an attractive potential, whilst already visited regions where given a repulsive potential. This way, the robot is driven toward regions of higher concentration and repulsed from regions it has already visited, avoiding wasted navigation efforts and local minima. The APF IPP relies on various coefficients that should be tuned based on the robot used and environment of operation. Outdoor experiments using a mini drone found that meaningful gas distribution maps were achieved more quickly when using the IPP in comparison to using a nonadaptive strategy. The exploitative tendency of the IPP was found to be beneficial for use with UAVs due to their limited battery resources.

Although a greedy IPP approach may allow for gas sources to be localized quickly, the quality of the overall gas distribution map may reduce. To promote more exploration while limiting unnecessary navigation efforts, Ercolani et al. (2022) proposed dividing the overall search space into clusters using the K-means algorithm and performing IPP within the cells of the clusters. For GDM, the 3D Kernel DM+V/W algorithm was used to compute online gas distribution maps and feed the IPP with updated information. The time allocated to exploring a cluster was dependent on the remaining flight time, number of unvisited clusters, and proportion of updated cells containing gas. This way, if the percentage of updated cells containing gas remained higher than a threshold, the robot would continue to explore the cluster until its allocated time ran out. On the contrary, if the percentage of updated cells counting gas remained low, the robot would be prompted to move to a new cell. This strategy ensures that the robot does not over-exploit one area, whilst promoting exploration to unvisited regions. Two common IPP planning methods were evaluated in wind tunnel experiments using a nano drone: entropy, and KL divergence. Both methods were found to provide similar levels of performance when using the clustered approach, however, both outperformed a nonadaptive lawnmower strategy by producing maps with less error and better coverage.

To account for obstacles within the search space, Rhodes et al. (2020) investigated the possibility of using IPP with GMRF. Since the connection relationship of GMRF nodes are defined within a Jacobian matrix, A^* search could be applied to find a distance metric between cells (nodes). This distance metric was used to provide a traversal cost, which was equivalent to the distance metric divided by the robot velocity, plus the sensing sample time (needed as sensors typically need to be stationary to get a representative time-averaged

value). As GMRF provides two outputs in the form of mean and uncertainty, the addition of the traversal cost gives three possible variables to be considered by the IPP reward function. Five potential IPP reward functions were proposed, and their performance was evaluated in CFD simulations of a source release in a cluttered environment. The best performing function was found to be a time-weighted joint uncertainty and concentration reward function, which was found to resolve an accurate distribution map in half the time of a nonadaptive strategy. Experiments in real environments are needed to further validate the proposed IPP.

As obstacles are accounted for within the graph-based structure of the GMRF algorithm, they do not need to be further considered by the IPP. GMRF is however a computationally expensive algorithm which would not be suited to robot platforms with limited onboard resources. Furthermore, as IPP requires real-time updates of the gas distribution map, robot progress maybe slowed down in large areas due to the longer computation time. This inspired Prabowo et al. (2022) to utilize a graph-based Kernel DM+V algorithm, where nodes have the attributes of gas concentration mean and variance, and edges represent traversable paths. The graph is built over free space with RRT during a "frontier exploration" phase. Free space is determined with a 2D occupancy map built online using SLAM. During this phase, the next goal position is set as the frontier node with the most information gain according to the occupancy map. If at any point, a node possesses a mean concentration and variance surpassing a threshold, the algorithm moves to a "gas exploitation" phase where it visits the nodes in the surrounding area to collect measurements. Once variance drops below a threshold (due to the increasing number of measurements), the robot switches back to frontier exploration. The algorithm was evaluated in simulations of an obstacle-rich environment featuring a gas source. It was found that the proposed algorithm could be tuned to balance exploration and exploitation by varying the concentration mean and variance thresholds. It would be difficult to select optimum values for these constants in real experiments, which currently limits the feasibility of the algorithm.

6.5 | Gas tomography

The GDM algorithms presented thus far make use of chemical sensors that can only provide local point measurements of gas concentration. Although complete coverage is not required, the process of gathering concentration data is time-consuming when the area of interest is very large. An alternative approach is to use the remote sensing capabilities of a TDLAS sensor (Section 2.3) to gather data without needing to travel to every measurement location. As long as the area of interest does not feature many obstacles that could obstruct the beam, the robot can travel to sparsely located waypoints to measure the chemical concentration of positions within a finite radius of the measurement point, depending on the range of the TDLAS laser.

The gas concentration recorded by the TDLAS sensor is an integral measurement rather than an exact concentration due to the output being made up of the sum of concentration of which the laser beam has traveled through. Therefore, information on the path traveled by the TDLAS beam is required alongside the integral concentration measurements to produce chemical distribution maps in a process is known as gas tomography (Price et al., 2001). Much of the research into the application of TDLAS sensors on mobile robots for the purpose of gas tomography has been conducted by Bennetts et al. (Bennetts et al., 2012, 2013; Trincavelli et al., 2012). They proposed a grid-based approach by dividing the area of interest into a lattice of cubic cells. The algorithm first decomposes the line integral measurements of the TDLAS sensor based on the number of cells that the laser has traveled through. This was derived by estimating the start and end point of the TDLAS beam using a 3D model of the exploration scene, created using Octomap (Wurm et al., 2010). The task is then formulated as estimating the vector of chemical concentrations which best explains the set of TDLAS measurements. To test the algorithm, an outdoor experiment was conducted where a mobile robot was made to collect TDLAS measurements within a decommissioned landfill site that featured a simulated methane leak. At various waypoints, a Pan-Tilt unit manipulated the TDLAS sensor into making scans of the exploration area. The resulting chemical distribution map showed a clear region of high concentration near the methane source, along with a distribution of methane in the area surrounding it. The results proved that the integral measurements of TDLAS sensors can be used for the purpose of chemical distribution mapping, allowing for a faster means of mapping chemical concentration in large outdoor spaces.

As gas distribution is solely modeled by the algorithm, the exact location of the source is slightly more difficult to interpret. For this reason, the algorithm was further improved to give a variance map along with the map of distribution (Bennetts et al., 2014). This was shown to give better estimates of source position in comparison to the mean distribution map. A further improvement was made in how the TDLAS beam was decomposed, by representing the TDLAS beam as a cone shape rather than an idealized straight line. This was found to significantly reduce estimation error in the produced mean maps. Recently smaller and lighter TDLAS sensors have been brought to the market which can be utilized by UAVs (Figure 9). Initially, the TDLAS sensors were used to give a concentration value in $ppm \cdot m$ for the area beneath the UAV, either by scanning the area below with a gimbal-mounted sensor (Neumann et al., 2017), or by using sensors in fixed positions (Emran et al., 2017). Tomography was first conducted with UAVs in Neumann et al. (2018), where the previously discussed grid-based tomography algorithm proposed by Bennetts et al. was applied. In outdoor experiments, a mini drone was made to stop at set waypoints to collect measurements. At each waypoint, a Pan-Tilt unit manipulated the TDLAS sensor into performing a sweep, where measurements were sampled periodically. Even though only five waypoints were visited during each trial, the sweep allowed for the concentration in many cells to be determined. The gas distribution maps showed a region of high concentration near the center line of the plume. A problem that was noted was the difficulty in localization due to the GPS being used, this in turn caused error in the produced

FIGURE 9 Small TDLAS sensor mounted to a UAV. Reproduced from Neumann et al. (2017). Licensed under CC BY 4.0 (https://creativecommons.org/licenses/by/4.0/). [Color figure can be viewed at wileyonlinelibrary.com]

distribution maps. For future improvements, the mini drone would require better localization capabilities, which in turn would allow for more accurate distribution mapping.

7 | DISCUSSION

Early research into GSL with mobile robots was focused almost solely on developing gradient-based chemical source localization algorithms to track chemical plumes to their source. The algorithms produced were able to successfully locate chemical sources in highly controlled experiments, but often failed when utilized in dynamic environments due to the realistic intermittency in plume concentration. Alternatively, probabilistic GSL algorithms have shown to provide clear performance improvements in more realistic scenarios. They are however greatly impacted by inaccurate modeling of the underlying ATD parameters, which emphasizes the importance of an accurate robot localization strategy when applied to real applications. Modern advances in GPS systems have however made this less of a problem, with centimeter accurate real-time kinematic GPS modules now relatively cheap and easily integrated on robotic platforms (Stangebye et al., 2020).

A limitation of current probabilistic algorithms can be found in the ATD models that they use, which often do not fully represent the real plume dispersal, especially in cluttered environments. There have however been attempts to consider the effect of obstacles on plume dispersal by combining path planning strategies with probabilistic GSL algorithms (Rhodes et al., 2021). However, there are few examples where such algorithms have been evaluated on real robots. Accurate CFD models are currently too computationally expensive to run online, and so most algorithms make use of simpler IP or GP plume models. Furthermore, although such models have been used successfully in outdoor trials (Hutchinson et al., 2019), robots must stop to take time-averaged sensor measurements which can greatly increase search time. This problem has been reduced by the proposal of various multirobot probabilistic GSL algorithms which allow for multiple areas to be sampled simultaneously by a team of robots. The number of real examples of multirobot cooperation in larger outdoor environments is fairly limited, arising from the difficulties introduced by the need for wireless communication between robots and bandwidth restrictions.

Alternatively, model-free chemical distribution mapping algorithms can be used for source localization which do not make assumptions of steady and uniform airflow. It should be reiterated however that GDM provides benefits beyond just source localization, with just some of the applications including mapping dust pollution in industrial settings (Bennetts et al., 2016; Schaffernicht et al., 2017), monitoring emissions from landfill sites with UGVs (Bennetts et al., 2013) and UAVs (Emran et al., 2017), mapping gas emissions from water treatment facilities (Burgués et al., 2021), and monitoring environmental variables in greenhouses with UAVs (Roldán et al., 2015). The Kernel DM+V GDM algorithm has been evaluated in various works, and provides benefits in terms of low computational complexity and the generation of both mean and variance maps. Variance maps have shown to be of great usefulness in determining source location, due to the fluctuations in concentration correlating well to source proximity (Fackrell & Robins, 1982; Justus et al., 2002; Mylne & Mason, 1991; Yee et al., 1994).

Many variations of the Kernel algorithm have also been proposed, including MC Kernel DM+V which makes use of an E-nose to discriminate and map multiple types of chemicals. However, Kernel GDM algorithms do not account for the effect of obstacles on the gas distribution. Recently, GMRF has been proposed to bridge this gap, by modeling the grid of the search space as a Markov random field. GMRF is computationally expensive compared to Kernel DM+V, as execution time is dependent on map size, which means that a trade-off may be necessary between execution time and cell size for monitoring larger areas. A recent direction for the field is the use of IPP alongside GDM, making it possible to build gas distribution maps in less time. Greedy approaches can, however, produce lower quality maps through seeking out only high regions of concentration, therefore a balanced approach is important to ensure that truthful representation of gas distribution are estimated. As the IPP relies on online computation of the gas distribution maps, the GDM algorithm used must be computationally lightweight, especially for use with robots with limited onboard resources.

It is clear that gas sensing with UAVs is a current and future trend for the field with the majority of recent works discussed in this review being based around UAV platforms. Although modifications have been proposed to reduce the effect of wake on the chemical sensor response, UAVs are still burdened by noisy sensor measurements, limited flight times, and payload capacity. For smaller nano drones, these constraints are even more predominant, requiring gas sensing to be done in motion to make sensing over larger volumes feasible (Burgués et al., 2019; Ercolani & Martinoli, 2020). Although this review has discussed a number of real-world experiments where 2D GSL and GDM have been tested with UAVs, the extension to 3D is still a very new and challenging direction, with only a few practical examples using UAVs found in literature. It is envisioned that many more examples will be presented in the future, requiring further modifications to limit the effects of wake on chemical sensor

measurements, and algorithms with less of a reliance on time-averaged measurements.

The use of TDLAS sensors has also become an emerging trend in the field of mobile robot chemical sensing. Through the use of gas tomography, the number of discrete sampling locations needed for producing chemical distribution maps can be massively reduced by manipulating the TDLAS beam to sample different directions from the same physical location. Smaller TDLAS sensors have allowed for mini drones to make use of their benefits, making it possible to sample large areas within their limited flight time (Emran et al., 2017). Furthermore, by sampling from a suitable altitude, TDLAS sensors allow for UAVs to take measurements without disrupting the chemical plume with turbulence caused by their downwash. However, TDLAS sensors are heavy and expensive, making them unsuitable for use with many UAV platforms.

8 | CONCLUSION

Recent advancements in both chemical sensing and mobile robot hardware have allowed for great progress to be made on the subject of gas source localization and mapping. A focus of future research will likely be on reducing the reliance of many GSL and GDM algorithms on time-averaged measurements, reducing search times and battery consumption in the process. In addition, the trend toward the use of UAVs in 3D is sure to become a dominant topic, requiring improved chemical sensors and signal processing capabilities to extract information from noisy measurements.

This survey has provided a broad overview of recent work on the subject of GSL and GDM with mobile robots. Current challenges and directions are discussed, providing a reference for future research.

ACKNOWLEDGEMENTS

The authors would like to acknowledge the support of the Future Manufacturing Research Institute, College of Engineering, Swansea University and Advanced Sustainable Manufacturing Technologies (ASTUTE 2022) project, which is partly funded from the EU's European Regional Development Fund through the Welsh European Funding Office, in enabling the research upon which this paper is based. Further information on ASTUTE can be found at www.astutewales.com.

CONFLICT OF INTEREST

The authors declare no conflict of interest.

ORCID

Adam Francis http://orcid.org/0000-0003-3302-2233
Shuai Li http://orcid.org/0000-0001-8316-5289
Christian Griffiths http://orcid.org/0000-0002-7054-6135
Johann Sienz http://orcid.org/0000-0003-3136-5718

REFERENCES

Abdullah, A.N., Kamarudin, K., Mamduh, S.M., Adom, A.H. & Juffry, Z.H.M. (2020) Effect of environmental temperature and humidity on different metal oxide gas sensors at various gas concentration levels. In: *IOP Conference Series: Materials Science and Engineering*. Vol. 864. IOP Publishing, p. 012152.

Ahmadou, D., Laref, R., Losson, E. & Siadat, M. (2017) Reduction of drift impact in gas sensor response to improve quantitative odor analysis. In: *2017 IEEE International Conference on Industrial Technology (ICIT)*. IEEE, pp. 928–933.

Anderson, G., Sheesley, C., Tolson, J., Wilson, E. & Tunstel, E. (2006) A mobile robot system for remote measurements of ammonia vapor in the atmosphere. In: *2006 IEEE International Conference on Systems, Man and Cybernetics*. Vol. 1. IEEE, pp. 241–246.

Anderson, G.T., Mahdi, S., Khidir, J., Wilson, E.W., et al. (2014) Field studies of a robot system to measure ground emissions of methane. In: *2014 IEEE International Conference on Systems, Man, and Cybernetics (SMC)*. IEEE, pp. 808–812.

Anderson, J.O., Thundiyil, J.G., & Stolbach, A. (2012) Clearing the air: a review of the effects of particulate matter air pollution on human health. *Journal of Medical Toxicology*, *8*(2), 166–175.

Arain, M.A., Hernandez Bennetts, V., Schaffernicht, E. & Lilienthal, A.J. (2021) Sniffing out fugitive methane emissions: autonomous remote gas inspection with a mobile robot. *The International Journal of Robotics Research*, *40* (4–5), 782–814.

Arellano, S.R., Liu, E., Wood, K., Aiuppa, A., Allan, A., Bitetto, M., Bobrowski, N., Carn, S.A., Clarke, R., Corrales, E., et al. (2019) UAV-based measurements of the high-altitude plume of Manam volcano. In: *AGU Fall Meeting Abstracts*. Vol. *2019*. pp. EP13A–02.

Arroyo, P., Gómez, J., Herrero, J.L. & Lozano, J. (2022) Electrochemical gas sensing module combined with unmanned aerial vehicles for air quality monitoring. *Sensors and Actuators B: Chemical*, *364*, 131815.

Asadi, S., Pashami, S., Loutfi, A. & Lilienthal, A.J. (2011) Td kernel DM. v: time-dependent statistical gas distribution modelling on simulated measurements. In: *AIP Conference Proceedings*. Vol. 1362. American Institute of Physics, pp. 281–282.

Bachrach, A., Prentice, S., He, R. & Roy, N. (2011) Range-robust autonomous navigation in GPS-denied environments. *Journal of Field Robotics*, *28* (5), 644–666.

Bailey, J.K., Willis, M.A. & Quinn, R. D. (2005) A multi-sensory robot for testing biologically-inspired odor plume tracking strategies. In: *Proceedings, 2005 IEEE/ASME International Conference on Advanced Intelligent Mechatronics*. IEEE, pp. 1477–1481.

Bellingham, J., Richards, A. & How, J.P. (2002) Receding horizon control of autonomous aerial vehicles. In: *Proceedings of the 2002 American Control Conference (IEEE Cat. No. CH37301)*. Vol. 5. IEEE, pp. 3741–3746.

Bennetts, V.H., Lilienthal, A.J., Khaliq, A.A., Sesé, V.P. & Trincavelli, M. (2012) Gasbot: a mobile robotic platform for methane leak detection and emission monitoring. In: *Workshop on Robotics for Environmental Monitoring at the IEEE/RSJ International Conference on Intelligent Robots and Systems*. Citeseer.

Bennetts, V.H., Lilienthal, A.J. & Trincavelli, M. (2012) Creating true gas concentration maps in presence of multiple heterogeneous gas sources. In: *Sensors, 2012 IEEE*. IEEE, pp. 1–4.

Bennetts, V.H., Schaffernicht, E., Lilienthal, A.J., Fan, H., Kucner, T.P., Andersson, L. & Johansson, A. (2016) Towards occupational health improvement in foundries through dense dust and pollution monitoring using a complementary approach with mobile and stationary sensing nodes. In: *2016 IEEE/RSJ International Conference on Intelligent Robots and Systems (IROS)*. IEEE, pp. 131–136.

Bennetts, V.H., Schaffernicht, E., Sese, V.P., Lilienthal, A.J. & Trincavelli, M. (2014) A novel approach for gas discrimination in natural environments with open sampling systems. In: *SENSORS, 2014 IEEE*. IEEE, pp. 2046–2049.

Bennetts, V.H., Schaffernicht, E., Stoyanov, T., Lilienthal, A.J. & Trincavelli, M. (2014) Robot assisted gas tomography-localizing methane leaks in outdoor environments. In: *2014 IEEE International Conference on Robotics and Automation (ICRA)*. IEEE, pp. 6362–6367.

Bennetts, V.M.H., Lilienthal, A.J., Khaliq, A.A., Sese, V.P. & Trincavelli, M. (2013) Towards real-world gas distribution mapping and leak localization using a mobile robot with 3d and remote gas sensing capabilities. In: *2013 IEEE International Conference on Robotics and Automation*. IEEE, pp. 2335–2340.

Bing, L., Qing-Hao, M., Jia-Ying, W., Biao, S. & Ying, W. (2015) Three-dimensional gas distribution mapping with a micro-drone. In: *2015 34th Chinese Control Conference (CCC)*. IEEE, pp. 6011–6015.

Bodin, B., Wagstaff, H., Saecdi, S., Nardi, L., Vespa, E., Mawer, J., Nisbet, A., Luján, M., Furber, S., Davison, A. J., (2018) Slambench2: multi-objective head-to-head benchmarking for visual SLAM. In: *2018 IEEE International Conference on Robotics and Automation (ICRA)*. IEEE, pp. 3637–3644.

Bourne, J.R., Goodell, M.N., He, X., Steiner, J.A. & Leang, K.K. (2020) Decentralized multi-agent information-theoretic control for target estimation and localization: finding gas leaks. *The International Journal of Robotics Research*, *39* (13), 1525–1548.

Bourne, J.R., Pardyjak, E.R. & Leang, K.K. (2019) Coordinated Bayesian-based bioinspired plume source term estimation and source seeking for mobile robots. *IEEE Transactions on Robotics*, *35* (4), 967–986.

Brooke-Holland, L. (2012) Unmanned aerial vehicles (drones): an introduction. House of Commons Library: London, UK.

Burgués, J., Esclapez, M.D., Doñate, S. & Marco, S. (2021) Rhinos: a lightweight portable electronic nose for real-time odor quantification in wastewater treatment plants. *Iscience*, *24* (12), 103371.

Burgués, J., Esclapez, M.D., Doñate, S., Pastor, L. & Marco, S. (2021) Aerial mapping of odorous gases in a wastewater treatment plant using a small drone. *Remote Sensing*, *13* (9), 1757.

Burgués, J., Hernández, V., Lilienthal, A.J. & Marco, S. (2019) Smelling nano aerial vehicle for gas source localization and mapping. *Sensors*, *19* (3), 478.

Burgues, J. & Marco, S. (2019) Wind-independent estimation of gas source distance from transient features of metal oxide sensor signals. *IEEE Access*, *7*, 140460–140469.

Burgués, J., Valdez, L. F. & Marco, S. (2019) High-bandwidth e-nose for rapid tracking of turbulent plumes. In: *2019 IEEE International Symposium on Olfaction and Electronic Nose (ISOEN)*. IEEE, pp. 1–3.

Butterfield, D. (2021) Market review of gas sensors for industrial applications.

Campos, C., Elvira, R., Rodríguez, J.J.G., Montiel, J.M. & Tardós, J.D. (2021) Orb-slam3: an accurate open-source library for visual, visual-inertial, and multimap slam. *IEEE Transactions on Robotics*, *37* (6), 1874–1890.

Castro, A., Magnezi, N., Sintayehu, B., Quinto, A. & Abshire, P. (2018) Odor source localization on a nano quadcopter. In: *2018 IEEE Biomedical Circuits and Systems Conference (BioCAS)*. IEEE, pp. 1–4.

Chang, D., Wu, W., Webster, D. R., Weissburg, M. J. & Zhang, F. (2013) A bio-inspired plume tracking algorithm for mobile sensing swarms in turbulent flow. In: *2013 IEEE International Conference on Robotics and Automation*. IEEE, pp. 921–926.

Chen, C.-C., Kuo, C.-T., Chen, S.-Y., Lin, C.-H., Chue, J.-J., Hsieh, Y.-J., Cheng, C.-W., Wu, C.-M. & Huang, C.-M. (2018) Calibration of low-cost particle sensors by using machine-learning method. In: *2018 IEEE Asia Pacific Conference on Circuits and Systems (APCCAS)*. IEEE, pp. 111–114.

Chen, W.-H., Rhodes, C. & Liu, C. (2021) Dual control for exploitation and exploration (DCEE) in autonomous search. *Automatica*, *133*, 109851.

Chen, X., Marjovi, A., Huang, J. & Martinoli, A. (2020) Particle source localization with a low-cost robotic sensor system: algorithmic design and performance evaluation. *IEEE Sensors Journal*, *20* (21), 13074–13085.

Chen, X.-x. & Huang, J. (2019) Odor source localization algorithms on mobile robots: a review and future outlook. *Robotics and Autonomous Systems*, *112*, 123–136.

Chen, Y., Anderson, G., Mahdi, S., Khidir, J. & Wilson, E. (2012) A proposed robotic air quality monitoring system. In: *World Automation Congress 2012*. IEEE, pp. 1–5.

Croizé, P., Archez, M., Boisson, J., Roger, T. & Monsegu, V. (2015) Autonomous measurement drone for remote dangerous source location mapping. *International Journal of Environmental Science and Development*, *6* (5), 391.

Dai, X.-Y., Wang, J.-Y. & Meng, Q.-H. (2019) An infotaxis-based odor source searching strategy for a mobile robot equipped with a TDLAS gas sensor. In: *2019 Chinese Control Conference (CCC)*. IEEE, pp. 4492–4497.

Dhariwal, A., Sukhatme, G.S. & Requicha, A.A. (2004) Bacterium-inspired robots for environmental monitoring. In: *IEEE International Conference on Robotics and Automation, 2004. Proceedings. ICRA'04 2004*. Vol. 2. IEEE, pp. 1436–1443.

DiCarlo, S. & Falasconi, M. (2012) *Drift correction methods for gas chemical sensors in artificial olfaction systems: techniques and challenges*. INTECH Open Access Publisher.

DiLello, E., Trincavelli, M., Bruyninckx, H. & De Laet, T. (2014) Augmented switching linear dynamical system model for gas concentration estimation with MOX sensors in an open sampling system. *Sensors*, *14* (7), 12533–12559.

Dillon, W.R. & Goldstein, M. (1984) *Multivariate analysis: Methods and applications*. New York: Wiley, 1984.

Do, S., Lee, M. & Kim, J.-S. (2020) The effect of a flow field on chemical detection performance of quadrotor drone. *Sensors*, *20* (11), 3262.

Dong, L., Tittel, F.K., Li, C., Sanchez, N.P., Wu, H., Zheng, C., Yu, Y., Sampaolo, A. & Griffin, R. J. (2016) Compact TDLAS based sensor design using interband cascade lasers for mid-IR trace gas sensing. *Optics Express*, *24* (6), A528–A535.

Duisterhof, B.P., Krishnan, S., Cruz, J.J., Banbury, C.R., Fu, W., Faust, A., de Croon, G.C. & Reddi, V.J. (2019) Learning to seek: autonomous source seeking with deep reinforcement learning onboard a nano drone microcontroller. Advance online publication. arXiv preprint arXiv:1909.11236.

Duisterhof, B.P., Li, S., Burgués, J., Reddi, V.J. & de Croon, G.C. (2021) Sniffy bug: A fully autonomous swarm of gas-seeking nano quadcopters in cluttered environments. In: *2021 IEEE/RSJ International Conference on Intelligent Robots and Systems (IROS)*. IEEE, pp. 9099–9106.

Durrant-Whyte, H. (2000) A beginner's guide to decentralised data fusion. Technical Document of Australian Centre for Field Robotics, University of Sydney, Australia, 1–27.

Eberhart, R. & Kennedy, J. (1995) A new optimizer using particle swarm theory. In: *MHS'95. Proceedings of the Sixth International Symposium on Micro Machine and Human Science*. IEEE, pp. 39–43.

Eberhart, R.C. & Shi, Y. (2000) Comparing inertia weights and constriction factors in particle swarm optimization. In: *Proceedings of the 2000 congress on evolutionary computation. CEC00 (Cat. No. 00TH8512)*. Vol. 1. IEEE, pp. 84–88.

Eberhart, R.C. & Shi, Y. (2001) Tracking and optimizing dynamic systems with particle swarms. In: *Proceedings of the 2001 Congress on Evolutionary Computation (IEEE Cat. No. 01TH8546)*. Vol. 1. IEEE, pp. 94–100.

Edwards, S., Rutkowski, A. J., Quinn, R.D. & Willis, M.A. (2005) Moth-inspired plume tracking strategies in three-dimensions. In: *Proceedings of the 2005 IEEE International Conference on Robotics and Automation*. IEEE, pp. 1669–1674.

Emery, R., Rahbar, F., Marjovi, A. & Martinoli, A. (2017) Adaptive lévy taxis for odor source localization in realistic environmental conditions. In: *2017 IEEE International Conference on Robotics and Automation (ICRA)*. IEEE, pp. 3552–3559.

Emran, B.J., Tannant, D.D. & Najjaran, H. (2017) Low-altitude aerial methane concentration mapping. *Remote Sensing*, *9* (8), 823.

Ercolani, C. & Martinoli, A. (2020) 3d odor source localization using a micro aerial vehicle: System design and performance evaluation. In: *2020 IEEE/RSJ International Conference on Intelligent Robots and Systems (IROS)*. IEEE, pp. 6194–6200.

Ercolani, C., Tang, L., Humne, A.A. & Martinoli, A. (2022) Clustering and informative path planning for 3d gas distribution mapping: algorithms and performance evaluation. *IEEE Robotics and Automation Letters*, *7* (2), 5310–5317.

Eu, K.S. & Yap, K.M. (2018) Chemical plume tracing: a three-dimensional technique for quadrotors by considering the altitude control of the robot in the casting stage. *International Journal of Advanced Robotic Systems*, *15* (1), 1729881418755877.

Fackrell, J. & Robins, A. (1982) Concentration fluctuations and fluxes in plumes from point sources in a turbulent boundary layer. *Journal of Fluid Mechanics*, *117*, 1–26.

Fan, H., Bennetts, V.H., Schaffernicht, E. & Lilienthal, A.J. (2016) Unsupervised gas discrimination in uncontrolled environments by exploiting density peaks. In: *2016 IEEE Sensors*. IEEE, pp. 1–3.

Fan, H., HernandezBennetts, V., Schaffernicht, E. & Lilienthal, A.J. (2019) Towards gas discrimination and mapping in emergency response scenarios using a mobile robot with an electronic nose. *Sensors*, *19* (3), 685.

Ferri, G., Caselli, E., Mattoli, V., Mondini, A., Mazzolai, B. & Dario, P. (2009) Spiral: A novel biologically-inspired algorithm for gas/odor source localization in an indoor environment with no strong airflow. *Robotics and Autonomous Systems*, *57* (4), 393–402.

Fjelsted, L., Christensen, A., Larsen, J., Kjeldsen, P. & Scheutz, C. (2019) Assessment of a landfill methane emission screening method using an unmanned aerial vehicle mounted thermal infrared camera—a field study. *Waste Management*, *87*, 893–904.

Fukazawa, Y. & Ishida, H. (2009) Estimating gas-source location in outdoor environment using mobile robot equipped with gas sensors and anemometer. In: *Sensors, 2009 IEEE*. IEEE, 6, pp. 1721–1724.

Gao, B., Li, H., Li, W. & Sun, F. (2016) 3D moth-inspired chemical plume tracking and adaptive step control strategy. *Adaptive Behavior*, *24* (1), 52–65.

Gentner, C. & Ulmschneider, M. (2017) Simultaneous localization and mapping for pedestrians using low-cost ultra-wideband system and gyroscope. In: *2017 International Conference on Indoor Positioning and Indoor Navigation (IPIN)*. IEEE, pp. 1–8.

Giernacki, W., Skwierczyński, M., Witwicki, W., Wroński, P. & Kozierski, P. (2017) Crazyflie 2.0 quadrotor as a platform for research and education in robotics and control engineering. In: *2017 22nd International Conference on Methods and Models in Automation and Robotics (MMAR)*. IEEE, pp. 37–42.

Goldenstein, C.S., Spearrin, R.M., Jeffries, J.B. & Hanson, R.K. (2017) Infrared laser-absorption sensing for combustion gases. *Progress in Energy and Combustion Science*, *60*, 132–176.

Gongora, A., Monroy, J. & Gonzalez-Jimenez, J. (2020) Joint estimation of gas and wind maps for fast-response applications. *Applied Mathematical Modelling*, *87*, 655–674.

Gonzalez-Jimenez, J., Monroy, J.G. & Blanco, J.L. (2011) The multi-chamber electronic nose—an improved olfaction sensor for mobile robotics. *Sensors*, *11* (6), 6145–6164.

Gosmann, J. & Opper, M. (2013) Gaussian processes for plume distribution estimation with UAVs.

Grasso, F. W. & Atema, J. (2002) Integration of flow and chemical sensing for guidance of autonomous marine robots in turbulent flows. *Environmental Fluid Mechanics*, *2* (1), 95–114.

Grasso, F.W., Basil, J.A. & Atema, J. (1998) Toward the convergence: robot and lobster perspectives of tracking odors to their source in the turbulent marine environment In: *Proceedings of the 1998 IEEE International Symposium on Intelligent Control (ISIC) held jointly with IEEE International Symposium on Computational Intelligence in Robotics and Automation (CIRA) Intell*. IEEE, pp. 259–264.

Gutierrez-Osuna, R. & Nagle, H.T. (1999) A method for evaluating data-preprocessing techniques for odour classification with an array of gas sensors. *IEEE Transactions on Systems, Man, and Cybernetics, Part B (Cybernetics)*, *29* (5), 626–632.

Hajieghrary, H., Hsieh, M.A. & Schwartz, I.B. (2016) Multi-agent search for source localization in a turbulent medium. *Physics Letters A*, *380* (20), 1698–1705.

Harvey, D.J., Lu, T.-F. & Keller, M.A. (2008) Comparing insect-inspired chemical plume tracking algorithms using a mobile robot. *IEEE Transactions on Robotics*, *24* (2), 307–317.

Hayes, A.T., Martinoli, A. & Goodman, R.M. (2002) Distributed odor source localization. *IEEE Sensors Journal*, *2* (3), 260–271.

He, X., Steiner, J.A., Bourne, J.R. & Leang, K.K. (2019) Gaussian-based kernel for multi-agent aerial chemical-plume mapping. In: *Dynamic Systems and Control Conference*. Vol. 59162. American Society of Mechanical Engineers, p.V003T21A004.

HernandezBennetts, V., Lilienthal, A. J., Neumann, P. & Trincavelli, M. (2012) Mobile robots for localizing gas emission sources on landfill sites: is bio-inspiration the way to go? *Frontiers in Neuroengineering*, *4*, 20.

HernandezBennetts, V., Schaffernicht, E., Pomareda, V., Lilienthal, A.J., Marco, S. & Trincavelli, M. (2014) Combining non selective gas sensors on a mobile robot for identification and mapping of multiple chemical compounds. *Sensors*, *14* (9), 17331–17352.

Hojaiji, H., Kalantarian, H., Bui, A.A., King, C.E. & Sarrafzadeh, M. (2017) Temperature and humidity calibration of a low-cost wireless dust sensor for real-time monitoring. In: *2017 IEEE sensors applications symposium (SAS)*. IEEE, pp. 1–6.

Hornung, A., Wurm, K.M., Bennewitz, M., Stachniss, C. & Burgard, W. (2013) Octomap: an efficient probabilistic 3d mapping framework based on octrees. *Autonomous Robots*, *34* (3), 189–206.

Hutchinson, M., Ladosz, P., Liu, C. & Chen, W.-H. (2019) Experimental assessment of plume mapping using point measurements from unmanned vehicles. In: *2019 International Conference on Robotics and Automation (ICRA)*. IEEE, pp. 7720–7726.

Hutchinson, M., Liu, C. & Chen, W.-H. (2018) Information-based search for an atmospheric release using a mobile robot: algorithm and experiments. *IEEE Transactions on Control Systems Technology*, *27* (6), 2388–2402.

Hutchinson, M., Liu, C. & Chen, W.-H. (2019) Source term estimation of a hazardous airborne release using an unmanned aerial vehicle. *Journal of Field Robotics*, *36* (4), 797–817.

Hutchinson, M., Liu, C., Thomas, P. & Chen, W.-H. (2019) UAV based hazmat response: information-theoretic hazardous source search and reconstruction.

Hutchinson, M., Liu, C., Thomas, P. & Chen, W.-H. (2019) Unmanned aerial vehicle-based hazardous materials response: information-theoretic hazardous source search and reconstruction. *IEEE Robotics & Automation Magazine*, *27* (3), 108–119.

Hutchinson, M., Oh, H. & Chen, W.-H. (2017) Adaptive Bayesian sensor motion planning for hazardous source term reconstruction. *IFAC-PapersOnLine*, *50* (1), 2812–2817.

Hutchinson, M., Oh, H. & Chen, W.-H. (2017) A review of source term estimation methods for atmospheric dispersion events using static or mobile sensors. *Information Fusion*, *36*, 130–148.

Hutchinson, M., Oh, H. & Chen, W.-H. (2018) Entrotaxis as a strategy for autonomous search and source reconstruction in turbulent conditions. *Information Fusion*, *42*, 179–189.

Ishida, H., Nakamoto, T. & Moriizumi, T. (1998) Remote sensing of gas/odor source location and concentration distribution using mobile system. *Sensors and Actuators B: Chemical*, *49* (1-2), 52–57.

Ishida, H., Nakayama, G., Nakamoto, T. & Moriizumi, T. (2005) Controlling a gas/odor plume-tracking robot based on transient responses of gas sensors. *IEEE Sensors Journal*, *5* (3), 537–545.

Ishida, H., Wada, Y. & Matsukura, H. (2012) Chemical sensing in robotic applications: a review. *IEEE Sensors Journal*, *12* (11), 3163–3173.

Iwaszenko, S., Kalisz, P., Słota, M. & Rudzki, A. (2021) Detection of natural gas leakages using a laser-based methane sensor and uav. *Remote Sensing*, *13* (3), 510.

Jatmiko, W., Pambuko, W., Mursanto, P., Muis, A., Kusumoputro, B., Sekiyama, K. & Fukuda, T. (2009) Localizing multiple odor sources in dynamic environment using ranged subgroup pso with flow of wind based on open dynamic engine library. In: *2009 International Symposium on Micro-NanoMechatronics and Human Science*. IEEE, pp. 602–607.

Jatmiko, W., Sekiyama, K. & Fukuda, T. (2007) A pso-based mobile robot for odor source localization in dynamic advection-diffusion with obstacles environment: theory, simulation and measurement. *IEEE Computational Intelligence Magazine*, *2* (2), 37–51.

Jayaratne, R., Liu, X., Thai, P., Dunbabin, M. & Morawska, L. (2018) The influence of humidity on the performance of a low-cost air particle mass sensor and the effect of atmospheric fog. *Atmospheric Measurement Techniques*, *11* (8), 4883–4890.

Jaynes, E.T. (2003) *Probability theory: The logic of science*. Cambridge University Press.

Jensen, D.D., Lucas, D.D., Lundquist, K.A. & Glascoe, L.G. (2019) Sensitivity of a Bayesian source-term estimation model to spatio-temporal sensor resolution. *Atmospheric Environment: X*, *3*, 100045.

Ji, Y., Chen, F., Chena, B., Wang, Y., Zhu, X. & He, H. (2021) Multi-robot collaborative source searching strategy in large-scale chemical clusters. *IEEE Sensors Journal*.

Jovašević-Stojanović, M., Davidović, M., Tasić, V., Bartoňová, A. & Ristovski, Z. (2017) Current status of applicability of low-cost particulate matter sensors for ambient air pollution and exposure assessment. In: *The Sixth International WeBIOPATR Workshop & Conference. Particulate Matter: Research and Management*. Vinca Institute of Nuclear Sciences, pp. 228–236.

Justus, K.A., Murlis, J., Jones, C. & Cardé, R.T. (2002) Measurement of odor-plume structure in a wind tunnel using a photoionization detector and a tracer gas. *Environmental Fluid Mechanics*, *2* (1), 115–142.

Kaelbling, L.P., Littman, M.L. & Cassandra, A.R. (1998) Planning and acting in partially observable stochastic domains. *Artificial intelligence*, *101* (1–2), 99–134.

Kailath, T. (1967) The divergence and Bhattacharyya distance measures in signal selection. *IEEE Transactions on Communication Technology*, *15* (1), 52–60.

Karpas, E.D., Shklarsh, A. & Schneidman, E. (2017) Information socialtaxis and efficient collective behavior emerging in groups of information-seeking agents. *Proceedings of the National Academy of Sciences of the United States of America*, *114* (22), 5589–5594.

Keats, A., Yee, E. & Lien, F.-S. (2007) Bayesian inference for source determination with applications to a complex urban environment. *Atmospheric Environment*, *41* (3), 465–479.

Kelly, K., Whitaker, J., Petty, A., Widmer, C., Dybwad, A., Sleeth, D., Martin, R. & Butterfield, A. (2017) Ambient and laboratory evaluation of a low-cost particulate matter sensor. *Environmental Pollution*, *221*, 491–500.

Kennedy, J. & Eberhart, R. (1995) Particle swarm optimization. In: *Proceedings of ICNN'95-international conference on neural networks*. Vol. 4. IEEE, pp. 1942–1948.

Kim, H. & Choi, Y. (2021) Self-driving algorithm and location estimation method for small environmental monitoring robot in underground mines. *Computer Modeling in Engineering & Sciences*, *127*, 943–964.

Korotcenkov, G. (2007) Metal oxides for solid-state gas sensors: what determines our choice? *Materials Science and Engineering: B*, *139* (1), 1–23.

Kroll, A., Baetz, W. & Peretzki, D. (2009) On autonomous detection of pressured air and gas leaks using passive IR-thermography for mobile robot application. In: *2009 IEEE International Conference on Robotics and Automation*. IEEE, pp. 921–926.

Kuantama, E., Tarca, R., Dzitac, S., Dzitac, I., Vesselenyi, T. & Tarca, I. (2019) The design and experimental development of air scanning using a sniffer quadcopter. *Sensors*, *19* (18), 3849.

Kuwana, Y., Shimoyama, I., Sayama, Y. & Miura, H. (1996) Synthesis of pheromone-oriented emergent behavior of a silkworm moth. In: *Proceedings of IEEE/RSJ International Conference on Intelligent Robots and Systems. IROS'96*. Vol. 3. IEEE, pp. 1722–1729.

Latif, R. & Saddik, A. (2019) Slam algorithms implementation in a UAV, based on a heterogeneous system: a survey. In: *2019 4th World Conference on Complex Systems (WCCS)*. IEEE, pp. 1–6.

Lee, H., Kang, J., Kim, S., Im, Y., Yoo, S. & Lee, D. (2020) Long-term evaluation and calibration of low-cost particulate matter (pm) sensor. *Sensors*, *20* (13), 3617.

Lee, K.-B., Kim, Y.-J. & Hong, Y.-D. (2018) Real-time swarm search method for real-world quadcopter drones. *Applied Sciences*, *8* (7), 1169.

Li, F., Meng, Q.-H., Bai, S., Li, J.-G. & Popescu, D. (2008) Probability-PSO algorithm for multi-robot based odor source localization in ventilated indoor environments. In: *International Conference on Intelligent Robotics and Applications*. Springer, pp. 1206–1215.

Li, J., Bi, Y., Li, K., Wang, K., Lin, F. & Chen, B.M. (2018) Accurate 3d localization for MAV swarms by UWB and imu fusion. In: *2018 IEEE 14th International Conference on Control and Automation (ICCA)*. IEEE, pp. 100–105.

Li, J.-G., Cao, M.-L. & Meng, Q.-H. (2019) Chemical source searching by controlling a wheeled mobile robot to follow an online planned route in outdoor field environments. *Sensors*, *19* (2), 426.

Li, J.-G., Meng, Q.-H., Wang, Y. & Zeng, M. (2011) Odor source localization using a mobile robot in outdoor airflow environments with a particle filter algorithm. *Autonomous Robots*, *30* (3), 281–292.

Li, S., Kong, R. & Guo, Y. (2014) Cooperative distributed source seeking by multiple robots: algorithms and experiments. *IEEE/ASME Transactions on Mechatronics*, *19* (6), 1810–1820.

Lilienthal, A. & Duckett, T. (2004) Building gas concentration gridmaps with a mobile robot. *Robotics and Autonomous Systems*, *48* (1), 3–16.

Lilienthal, A. & Duckett, T. (2004) Experimental analysis of gas-sensitive braitenberg vehicles. *Advanced Robotics*, *18* (8), 817–834.

Lilienthal, A., Reimann, D. & Zell, A. (2003) Gas source tracing with a mobile robot using an adapted moth strategy. In: Autonome Mobile Systeme 2003, pp. 150–160.

Lilienthal, A., Zell, A., Wandel, M. & Weimar, U. (2001) Sensing odour sources in indoor environments without a constant airflow by a mobile robot. In: *Proceedings 2001 ICRA, IEEE International Conference on Robotics and Automation (Cat. No. 01CH37164)*. Vol. 4. IEEE, pp. 4005–4010.

Lilienthal, A.J., Loutfi, A. & Duckett, T. (2006) Airborne chemical sensing with mobile robots. *Sensors*, *6* (11), 1616–1678.

Lilienthal, A.J., Reggente, M., Trincavelli, M., Blanco, J.L. & Gonzalez, J. (2009) A statistical approach to gas distribution modelling with mobile robots-the kernel dm. v algorithm. In: *2009 IEEE/RSJ International Conference on Intelligent Robots and Systems*. IEEE, pp. 570–576.

Lindley, D.V. (1956) On a measure of the information provided by an experiment. *The Annals of Mathematical Statistics*, *27*, 986–1005.

Liu, H.-Y., Schneider, P., Haugen, R. & Vogt, M. (2019)Performance assessment of a low-cost pm2. 5 sensor for a near four-month period in Oslo, Norway. *Atmosphere*, *10* (2), 41.

Lochmatter, T., Göl, E. A., Navarro, I. & Martinoli, A. (2013) A plume tracking algorithm based on crosswind formations. In: *Distributed Autonomous Robotic Systems*, *83*, pp. 91–102.

Lu, T.-F. (2013) Indoor odour source localisation using robot: initial location and surge distance matter? *Robotics and Autonomous Systems*, *61* (6), 637–647.

Maag, B., Zhou, Z. & Thiele, L. (2018) A survey on sensor calibration in air pollution monitoring deployments. *IEEE Internet of Things Journal*, *5* (6), 4857–4870.

Macedo, J., Marques, L. & Costa, E. (2019) A comparative study of bio-inspired odour source localisation strategies from the state-action perspective. *Sensors*, *19* (10), 2231.

Maes, P., Mataric, M.J., Meyer, J.-A., Pollack, J. & Wilson, S.W. (1996) Locating odor sources in turbulence with a lobster inspired robot.

Magalhães, H., Baptista, R., Macedo, J. & Marques, L. (2020) Towards fast plume source estimation with a mobile robot. *Sensors*, *20* (24), 7025.

Mamduh, S.M., Kamarudin, K., Saad, S.M., Shakaff, A.Y.M., Zakaria, A. & Abdullah, A. H. (2013) Braitenberg swarm vehicles for odour plume tracking in laminar airflow. In: *2013 IEEE Symposium on Computers & Informatics (ISCI)*. IEEE, pp. 1–6.

Marchant, R. & Ramos, F. (2012) Bayesian optimisation for intelligent environmental monitoring. In: *2012 IEEE/RSJ international conference on intelligent robots and systems*. IEEE, pp. 2242–2249.

MartinMoraud, E. & Martinez, D. (2010) Effectiveness and robustness of robot infotaxis for searching in dilute conditions. *Frontiers in neurorobotics*, *4*, 1.

Martinez, C.J.M., Salguero, R.C., Palomares, R. & Cornejo, J. (2020) Mechatronics development of terrestrial mobile robot for exploring and monitoring environmental parameters at mine analogue sites using IoT platform. In: *2020 IEEE XXVII International Conference on Electronics, Electrical Engineering and Computing (INTERCON)*. IEEE, pp. 1–4.

Masiero, A., Fissore, F., Antonello, R., Cenedese, A. & Vettore, A. (2019) A comparison of UWB and motion capture UAV indoor positioning. *The International Archives of Photogrammetry, Remote Sensing and Spatial Information Sciences*, *42*, 1695–1699.

Meng, Q.-H., Yang, W.-X., Wang, Y. & Zeng, M. (2011) Collective odor source estimation and search in time-variant airflow environments using mobile robots. *Sensors*, *11* (11), 10415–10443.

Mishra, V., Dwivedi, R. & Das, R. (2013) Classification of gases/odors using dynamic responses of thick film gas sensor array. *IEEE Sensors Journal*, *13*(12), 4924–4930.

Mishra, V., Dwivedi, R. & Das, R. (2013) Quantification of individual gases/odors using dynamic responses of gas sensor array with asm feature technique. *IEEE Sensors Journal*, *14*(4), 1006–1011.

Mokrani, H., Lounas, R., Bennai, M.T., Salhi, D.E. & Djerbi, R. (2019) Air quality monitoring using iot: A survey. In: *2019 IEEE International Conference on Smart Internet of Things (SmartIoT)*. IEEE, pp. 127–134.

Monroy, J.G., Blanco, J.-L. & Jiménez, J.G. (2016) Time-variant gas distribution mapping with obstacle information. *Autonomous Robots*, *40* (1), 1–16.

Monroy, J.G., Jaimez, M. & Gonzalez-Jimenez, J. (2017) Online estimation of 2d wind maps for olfactory robots. In: *2017 ISOCS/IEEE International Symposium on Olfaction and Electronic Nose (ISOEN)*. IEEE, pp. 1–3.

Monroy, J.G., Lilienthal, A.J., Blanco, J.-L., Gonzalez-Jimenez, J. & Trincavelli, M. (2013) Probabilistic gas quantification with MOX sensors in open sampling systems—a Gaussian process approach. *Sensors and Actuators B: Chemical*, *188*, 298–312.

Mooney, D., Willis, P. & Stevenson, K. (2006) *A guide for local authorities purchasing air quality monitoring equipment*. AEA Technology Plc: Harwell, UK.

Mylne, K.R. & Mason, P. (1991) Concentration fluctuation measurements in a dispersing plume at a range of up to 1000 m. *Quarterly Journal of the Royal Meteorological Society*, *117* (497), 177–206.

Nathan, B.J., Golston, L.M., O'Brien, A.S., Ross, K., Harrison, W.A., Tao, L., Lary, D.J., Johnson, D.R., Covington, A.N., Clark, N.N., et al. (2015) Near-field characterization of methane emission variability from a compressor station using a model aircraft. *Environmental science & technology*, *49* (13), 7896–7903.

Neumann, P.P. (2013) Gas source localization and gas distribution mapping with a micro-drone.

Neumann, P.P., Asadi, S., Bennetts, V.H., Lilienthal, A.J. & Bartholmai, M. (2013) Monitoring of CCS areas using micro unmanned aerial vehicles (MUAVs). *Energy Procedia*, *37*, 4182–4190.

Neumann, P.P., Asadi, S., Lilienthal, A.J., Bartholmai, M. & Schiller, J.H. (2012) Autonomous gas-sensitive microdrone: wind vector estimation and gas distribution mapping. *IEEE Robotics & Automation Magazine*, *19* (1), 50–61.

Neumann, P.P., Asadi, S., Lilienthal, A.J., Bartholmai, M. & Schiller, J.H. (2012) Wind vector estimation and gas distribution mapping. *Journal of IEEE Robotics and Automation Magazine*, *19*, 6.

Neumann, P.P., Bennetts, M. & Bartholmai, I.M. (2012) Adaptive gas source localization strategies and gas distribution mapping using a gas-sensitive micro-drone. *Technology (BMWi)*, *4* (5), 6.

Neumann, P.P., Hüllmann, D. & Bartholmai, M. (2019) Concept of a gas-sensitive nano aerial robot swarm for indoor air quality monitoring. *Materials Today: Proceedings*, *12*, 470–473.

Neumann, P.P., Hüllmann, D., Krentel, D., Kluge, M., Kohlhoff, H. & Lilienthal, A.J. (2018) Gas tomography up in the air In: *2018 IEEE SENSORS*. IEEE, pp. 1–4.

Neumann, P.P., Kohlhoff, H., Hüllmann, D., Krentel, D., Kluge, M., Dzierliński, M., Lilienthal, A.J. & Bartholmai, M. (2019) Aerial-based gas tomography-from single beams to complex gas distributions. *European Journal of Remote Sensing*, *52* (5), 2–16.

Neumann, P.P., Kohlhoff, H., Hüllmann, D., Lilienthal, A.J. & Kluge, M. (2017) Bringing mobile robot olfaction to the next dimension-uav-based remote sensing of gas clouds and source localization. In: *2017 IEEE International Conference on Robotics and Automation (ICRA)*. IEEE, pp. 3910–3916.

Nguyen, T.M., Zaini, A.H., Guo, K. & Xie, L. (2016) An ultra-wideband-based multi-UAV localization system in gps-denied environments. In: *2016 International Micro Air Vehicles Conference*. Vol. 6. pp. 1–15.

Nimsuk, N. (2014) Enhancement of classification performance of an electronic nose using short-time fourier transform. In: *2014 International Electrical Engineering Congress (iEECON)*. IEEE, pp. 1–4.

Ojeda, P., Monroy, J. & Gonzalez-Jimenez, J. (2021) Information-driven gas source localization exploiting gas and wind local measurements for autonomous mobile robots. *IEEE Robotics and Automation Letters*, *6* (2), 1320–1326.

Patel, N.D., Fales, W.D. & Farrell, R.N. (2009) The use of a photoionization detector to detect harmful volatile chemicals by emergency personnel. *Open Access Emergency Medicine: OAEM*, *1*, 5.

Peterson, P.J., Aujla, A., Grant, K.H., Brundle, A.G., Thompson, M.R., Vande Hey, J. & Leigh, R.J. (2017) Practical use of metal oxide semiconductor gas sensors for measuring nitrogen dioxide and ozone in urban environments. *Sensors*, *17* (7), 1653.

Prabowo, Y.A., Trilaksono, B.R., Hidayat, E.M. & Yuliarto, B. (2022) Utilizing a rapidly exploring random tree for hazardous gas exploration in a large unknown area. *IEEE Access*, *10*, 15336–15347.

Price, P.N., Fischer, M.L., Gadgil, A.J. & Sextro, R.G. (2001) An algorithm for real-time tomography of gas concentrations, using prior information about spatial derivatives. *Atmospheric Environment*, *35* (16), 2827–2835.

Puschita, E., Simedroni, R., Palade, T., Codau, C., Vos, S., Ratiu, V. & Ratiu, O. (2020) Performance evaluation of the uwb-based cds indoor positioning solution. In: *2020 International Workshop on Antenna Technology (iWAT)*. IEEE, pp. 1–4.

Rahbar, F., Marjovi, A., Kibleur, P. & Martinoli, A. (2017) A 3-d bio-inspired odor source localization and its validation in realistic environmental conditions. In: *2017 IEEE/RSJ International Conference on Intelligent Robots and Systems (IROS)*. IEEE, pp. 3983–3989.

Rahbar, F., Marjovi, A. & Martinoli, A. (2019a) An algorithm for odor source localization based on source term estimation. In: *2019 International Conference on Robotics and Automation (ICRA)*. IEEE, pp. 973–979.

Rahbar, F., Marjovi, A. & Martinoli, A. (2019b) Design and performance evaluation of an algorithm based on source term estimation for odor source localization. *Sensors*, *19* (3), 656.

Rahbar, F. & Martinoli, A. (2020)A distributed source term estimation algorithm for multi-robot systems. In: *2020 IEEE International Conference on Robotics and Automation (ICRA)*. IEEE, pp. 5604–5610.

Rao, K.S. (2007) Source estimation methods for atmospheric dispersion. *Atmospheric Environment*, *41* (33), 6964–6973.

Rasmussen, C.E. (2003) Gaussian processes in machine learning. In: *Summer School on Machine Learning*. Springer, pp. 63–71.

Reggente, M. & Lilienthal, A.J. (2009) Three-dimensional statistical gas distribution mapping in an uncontrolled indoor environment. In: *AIP Conference Proceedings*. Vol. 1137. American Institute of Physics, pp. 109–112.

Reggente, M. & Lilienthal, A.J. (2009) Using local wind information for gas distribution mapping in outdoor environments with a mobile robot. In: *Sensors, 2009 IEEE*. IEEE, pp. 1715–1720.

Reggente, M. & Lilienthal, A.J. (2010) The 3d-kernel dm. v/w algorithm: using wind information in three dimensional gas distribution modelling with a mobile robot. In: *SENSORS 2010 IEEE*. IEEE, pp. 999–1004.

Ren, H., Zhao, Y., Xiao, W. & Hu, Z. (2019) A review of uav monitoring in mining areas: current status and future perspectives. *International Journal of Coal Science & Technology*, *6* (3), 320–333.

Ren, W., Beard, R.W. & Atkins, E.M. (2007) Information consensus in multivehicle cooperative control. *IEEE Control Systems Magazine*, *27* (2), 71–82.

Rhodes, C., Liu, C. & Chen, W.-H. (2020) Informative path planning for gas distribution mapping in cluttered environments. In: *2020 IEEE/RSJ International Conference on Intelligent Robots and Systems (IROS)*. IEEE, pp. 6726–6732.

Rhodes, C., Liu, C. & Chen, W.-H. (2022) Autonomous source term estimation in unknown environments: from a dual control concept to UAV deployment. *IEEE Robotics and Automation Letters*.

Rhodes, C., Liu, C., Westoby, P. & Chen, W.-H. (2021) Autonomous search of an airborne release in urban environments using informed tree planning. Advance online publication. arXiv preprint arXiv:2109.03542.

Ristic, B., Angley, D., Moran, B. & Palmer, J.L. (2017) Autonomous multi-robot search for a hazardous source in a turbulent environment. *Sensors*, *17* (4), 918.

Ristic, B., Gilliam, C., Moran, W. & Palmer, J.L. (2020) Decentralised multi-platform search for a hazardous source in a turbulent flow. *Information Fusion*, *58*, 13–23.

Ristic, B., Skvortsov, A. & Gunatilaka, A. (2016) A study of cognitive strategies for an autonomous search. *Information Fusion*, *28*, 1–9.

Ristic, B., Skvortsov, A. & Walker, A. (2014) Autonomous search for a diffusive source in an unknown structured environment. *Entropy*, *16* (2), 789–813.

Roberts, P.J. & Webster, D.R. (2002) *Turbulent diffusion*. ASCE Press, Reston, VA.

Rodriguez, A. & Laio, A. (2014). Clustering by fast search and find of density peaks. *Science*, *344* (6191), 1492–1496.

Rodríguez, J.D., Gómez-Ullate, D. & Mejía-Monasterio, C. (2014) Limits on the performance of infotaxis under inaccurate modelling of the environment. arXiv preprint arXiv:1408.1873.

Rodríguez, J.D., Gómez-Ullate, D. & Mejía-Monasterio, C. (2017) On the performance of blind-infotaxis under inaccurate modeling of the environment. *The European Physical Journal Special Topics*, *226* (10), 2407–2420.

Roldán, J.J., Joossen, G., Sanz, D., DelCerro, J. & Barrientos, A. (2015) Mini-UAV based sensory system for measuring environmental variables in greenhouses. *Sensors*, *15* (2), 3334–3350.

Rossi, M. & Brunelli, D. (2017) Gas sensing on unmanned vehicles: challenges and opportunities. In: 2017 New Generation of CAS (NGCAS). IEEE, pp. 117–120.

Rossi, M., Brunelli, D., Adami, A., Lorenzelli, L., Menna, F. & Remondino, F. (2014). Gas-drone: Portable gas sensing system on uavs for gas leakage localization. In: *Sensors, 2014 IEEE*. IEEE, pp. 1431–1434.

Rozas, R., Morales, J. & Vega, D. (1991) Artificial smell detection for robotic navigation. In: *Fifth International Conference on Advanced Robotics' Robots in Unstructured Environments*. IEEE, pp. 1730–1733.

Ruddick, J., Marjovi, A., Rahbar, F. & Martinoli, A. (2018) Design and performance evaluation of an infotaxis-based three-dimensional algorithm for odor source localization. In: *2018 IEEE/RSJ International Conference on Intelligent Robots and Systems (IROS)*. IEEE, pp. 1413–1420.

Russell, R.A., Bab-Hadiashar, A., Shepherd, R.L. & Wallace, G.G. (2003) A comparison of reactive robot chemotaxis algorithms. *Robotics and Autonomous Systems*, *45* (2), 83–97.

Rutkowski, A.J., Edwards, S., Willis, M.A., Quinn, R.D. & Causey, G.C. (2004) A robotic platform for testing moth-inspired plume tracking strategies. In: *IEEE International Conference on Robotics and Automation, 2004. Proceedings. ICRA'04. 2004*. Vol. 4. IEEE, pp. 3319–3324.

Santana, L.V., Brandao, A.S. & Sarcinelli-Filho, M. (2015) Outdoor waypoint navigation with the ar. drone quadrotor. In: *2015 International Conference on Unmanned Aircraft Systems (ICUAS)*. IEEE, pp. 303–311.

Schaffernicht, E., Bennetts, V.H. & Lilienthal, A.J. (2017) Mobile robots for learning spatio-temporal interpolation models in sensor networks–the echo state map approach. In: *2017 IEEE International Conference on Robotics and Automation (ICRA)*. IEEE, pp. 2659–2665.

Sebastiani, P. & Wynn, H.P. (2000) Maximum entropy sampling and optimal Bayesian experimental design, *Journal of the Royal Statistical Society: Series B (Statistical Methodology)*, *62* (1), 145–157.

Shigaki, S., Fikri, M. R. & Kurabayashi, D. (2018) Design and experimental evaluation of an odor sensing method for a pocket-sized quadcopter. *Sensors*, *18* (11), 3720.

Shraiman, B. I. & Siggia, E. D. (2000) Scalar turbulence. *Nature*, *405* (6787), 639–646.

Siqi, Z., Rongxin, C. & Demin, X. (2012) Effectiveness of infotaxis algorithm for searching in dilute conditions. In: *Proceedings of the 31st Chinese Control Conference*. IEEE, pp. 5048–5053.

Smola, A.J. & Bartlett, P.L. (2001) Sparse greedy Gaussian process regression. In: *Advances in Neural Information Processing Systems*, pp. 619–625.

Spinelle, L., Gerboles, M., Kok, G., Persijn, S. & Sauerwald, T. (2017) Review of portable and low-cost sensors for the ambient air monitoring of benzene and other volatile organic compounds. *Sensors*, *17* (7), 1520.

Stachniss, C., Plagemann, C. & Lilienthal, A.J. (2009) Learning gas distribution models using sparse Gaussian process mixtures. *Autonomous Robots*, *26* (2), 187–202.

Stachniss, C., Plagemann, C., Lilienthal, A.J. & Burgard, W. (2008) Gas distribution modeling using sparse gaussian process mixture models. In: *International Conference on Robotics Science and Systems, Robotics: science and systems, 2008, Zürich, Switzerland, June 25–28, 2008*. Vol. 4. MIT Press, pp. 310–317.

Stangebye, T., Mohr, T., Vallenti, A., Grauff, M. & Koziol, S. (2020) Custom real-time-kinematics positioning system testbed for mobile robot localization. In: *2020 IEEE 14th Dallas Circuits and Systems Conference (DCAS)*. IEEE, pp. 1–4.

Steiner, J.A., Bourne, J.R., He, X., Cropek, D.M. & Leang, K.K. (2019) Chemical-source localization using a swarm of decentralized unmanned aerial vehicles for urban/suburban environments. In: *Dynamic Systems and Control Conference*. Vol. 59162. American Society of Mechanical Engineers, pp. V003T21A006.

Steinfeld, J.I. (1998) Atmospheric chemistry and physics: from air pollution to climate change. *Environment: Science and Policy for Sustainable Development*, *40* (7), 26.

Takei, Y., Shimizu, Y., Hirasawa, K. & Nanto, H. (2014) Braitenbergas vehicle-like odor plume tracking robot. In: *2014 IEEE*. IEEE, pp. 1276–1279.

Terutsuki, D., Uchida, T., Fukui, C., Sukekawa, Y., Okamoto, Y. & Kanzaki, R. (2021) Real-time odor concentration and direction recognition for efficient odor source localization using a small bio-hybrid drone. *Sensors and Actuators B: Chemical*, *339*, 129770.

Trincavelli, M. (2011) Gas discrimination for mobile robots. *KI-Künstliche Intelligenz*, *25* (4), 351–354.

Trincavelli, M., Bennetts, V.H. & Lilienthal, A.J. (2012) A least squares approach for learning gas distribution maps from a set of integral gas concentration measurements obtained with a tdlas sensor. In: *Sensors, 2012 IEEE*. IEEE, pp. 1–4.

Tseng, L.Y. & Yang, S.B. (2000) A genetic clustering algorithm for data with non-spherical-shape clusters. *Pattern Recognition*, *33* (7), 1251–1259.

ur Rehman, A. & Bermak, A. (2018) Concentration estimation of industrial gases for electronic nose applications. In: *2018 30th International Conference on Microelectronics (ICM)*. IEEE, pp. 13–16.

van Well, B., Murray, S., Hodgkinson, J., Pride, R., Strzoda, R., Gibson, G. & Padgett, M. (2005) An open-path, hand-held laser system for the detection of methane gas. *Journal of Optics A: Pure and Applied Optics*, *7* (6), S420.

Vergassola, M., Villermaux, E. & Shraiman, B. I. (2007) Infotaxis' as a strategy for searching without gradients. *Nature*, *445* (7126), 406–409.

Villa, T.F., Salimi, F., Morton, K., Morawska, L. & Gonzalez, F. (2016) Development and validation of a UAV based system for air pollution measurements. *Sensors*, *16* (12), 2202.

Wandel, M., Weimar, U., Lilienthal, A. & Zell, A. (2001) Leakage localisation with a mobile robot carrying chemical sensors. In: *ICECS 2001. 8th IEEE International Conference on Electronics, Circuits and Systems (Cat. No. 01EX483)*. Vol. 3. IEEE, pp. 1247–1250.

Waphare, S., Gharpure, D., Shaligram, A. & Botre, B. (2010) Implementation of 3-nose strategy in odor plume-tracking algorithm. In: *2010 International Conference on Signal Acquisition and Processing*. IEEE, pp. 337–341.

Wei, G., Gardner, J.W., Cole, M. & Xing, Y. (2016)Multi-sensor module for a mobile robot operating in harsh environments. In: *2016 IEEE SENSORS*. IEEE, pp. 1–3.

Wiedemann, T., Lilienthal, A.J. & Shutin, D. (2019) Analysis of model mismatch effects for a model-based gas source localization strategy incorporating advection knowledge. *Sensors*, *19* (3), 520.

Wiedemann, T., Manss, C. & Shutin, D. (2018) Multi-agent exploration of spatial dynamical processes under sparsity constraints. *Autonomous Agents and Multi-Agent Systems*, *32* (1), 134–162.

Wiedemann, T., Manss, C., Shutin, D., Lilienthal, A.J., Karolj, V. & Viseras, A. (2017) Probabilistic modeling of gas diffusion with partial differential equations for multi-robot exploration and gas source localization. In: *2017 European Conference on Mobile Robots (ECMR)*. IEEE, pp. 1–7.

Wiedemann, T., Shutin, D., Hernandez, V., Schaffernicht, E. & Lilienthal, A.J. (2017) Bayesian gas source localization and exploration with a multi-robot system using partial differential equation based modeling. In: *2017 ISOCS/IEEE International Symposium on Olfaction and Electronic Nose (ISOEN)*. IEEE, pp. 1–3.

Wiedemann, T., Shutin, D. & Lilienthal, A.J. (2021) Experimental validation of domain knowledge assisted robotic exploration and source localization. In: *2021 IEEE International Conference on Autonomous Systems (ICAS)*. IEEE, pp. 1–5.

Winkvist, S., Rushforth, E. & Young, K. (2013) Towards an autonomous indoor aerial inspection vehicle. Industrial Robot: An International Journal.

Wurm, K.M., Hornung, A., Bennewitz, M., Stachniss, C. & Burgard, W. (2010). Octomap: a probabilistic, flexible, and compact 3d map representation for robotic systems. In: *Proceedings of the ICRA 2010 Workshop on Best Practice in 3D Perception and Modeling for Mobile Manipulation*. Vol. 2.

Xing, Y., Vincent, T. A., Cole, M., Gardner, J.W., Fan, H., Bennetts, V.H., Schaffernicht, E. & Lilienthal, A. J. (2017). Mobile robot multi-sensor unit for unsupervised gas discrimination in uncontrolled environments. In: *2017 IEEE SENSORS*. pp. 1–3.

Yang, B. & Yang, E. (2021) A survey on radio frequency based precise localisation technology for UAV in GPS-denied environment. *Journal of Intelligent & Robotic Systems*, *103* (3), 1–30.

Yang, T., Li, P., Zhang, H., Li, J. & Li, Z. (2018) Monocular vision slam-based UAV autonomous landing in emergencies and unknown environments. *Electronics*, *7* (5), 73.

Yee, E., Chan, R., Kosteniuk, P., Chandler, G., Biltoft, C. & Bowers, J. (1994) Experimental measurements of concentration fluctuations and scales in a dispersing plume in the atmospheric surface layer obtained using a very fast response concentration detector. *Journal of Applied Meteorology and Climatology*, *33* (8), 996–1016.

Yuan, H., Xiao, C., Wang, Y., Peng, X., Wen, Y. & Li, Q. (2020) Maritime vessel emission monitoring by an UAV gas sensor system. *Ocean Engineering*, *218*, 108206.

Zhang, J., Campbell, J.F., Sweeney II, D.C. & Hupman, A.C. (2021) Energy consumption models for delivery drones: a comparison and assessment. *Transportation Research Part D: Transport and Environment*, *90*, 102668.

Zhang, S., Xia, X., Xie, C., Cai, S., Li, H. & Zeng, D. (2009) A method of feature extraction on recovery curves for fast recognition application with metal oxide gas sensor array. *IEEE Sensors Journal*, *9* (12), 1705–1710.

Zhang, S., Xie, C., Zeng, D., Li, H., Bai, Z. & Cai, S. (2008) A method of feature extraction from the desorption part of MOX's response curves to gases. *IEEE Sensors Journal*, *8* (11), 1816–1823.

Zhou, J.-y., Li, J.-g. & Cui, S.-g. (2015) A bionic plume tracing method with a mobile robot in outdoor time-varying airflow environment. In: *2015 IEEE International Conference on Information and Automation*. IEEE, pp. 2351–2355.

How to cite this article: Francis, A., Li, S., Griffiths, C. & Sienz, J. (2022) Gas source localisation and mapping with mobile robots: A review. *Journal of Field Robotics*, 1–33. https://doi.org/10.1002/rob.22109